Ocean tides in the Weddell Sea: new observations on the Filchner-Ronne and Larsen C ice shelves and model validation

Matt A. King[1], Laurie Padman[2], Keith Nicholls[3], Peter J. Clarke[1], G. Hilmar Gudmundsson[3], Bernd Kulessa[4], Andrew Shepherd[5], Noel Gourmelen[5]

1. School of Civil Engineering and Geosciences, Cassie Building, Newcastle University, Newcastle upon Tyne, NE1 7RU, UK
2. Earth & Space Research, 3350 SW Cascade Ave, Corvallis, OR 97333-1536, Oregon, USA
3. British Antarctic Survey, Natural Environment Research Council, Madingley Road, Cambridge CB3 0ET, UK
4. College of Science, Swansea University, Singleton Park, Swansea SA2 8PP, UK
5. School of Earth and Environment, The University of Leeds, Leeds, LS2 9JT, UK

King, M. A., L. Padman, K. Nicholls, P. J. Clarke, G. H. Gudmundsson, B. Kulessa, and A. Shepherd (2011), Ocean tides in the Weddell Sea: New observations on the Filchner-Ronne and Larsen C ice shelves and model validation, J. Geophys. Res., 116, C06006, doi:10.1029/2011JC006949

Abstract

Ocean tides under the large Weddell Sea ice shelves are among the least well observed on Earth. Here we present new, spatially extensive observations of the vertical tidal motion of the Filchner-Ronne and Larsen C ice shelves using Global Positioning System (GPS) data spanning a few weeks to years. We pay particular attention to the major tidal constituents (M2, S2, O1, K1) as well as important GRACE aliasing periods (K2 and S1). We compare the estimated constituents with recent global and regional tide models and find that no single model is the most accurate across all constituents or ice shelves. The root-sum-square errors

are 7-8 cm (CATS2008a and TPXO7.2) and 11-12 cm (GOT4.7 and FES2004) with the energetic M2 (RMSE=4-8 cm) and S2 (4-5 cm) generally dominating these statistics. The FES2004 K1 is particularly inaccurate near the Larsen C Ice Shelf, with errors approaching 20 cm, meaning that GRACE Release 4 estimates of mass change in the northern Antarctic Peninsula will be biased. We find tidal energy at 3, 4, 5, 6 and, weakly, at 7 cycles per day at all of our sites. The largest amplitudes within these bands are at M4, MO3 and SP3 and approach 30 mm, although significant spatial variations exist. We show that they generally do not appear to originate in areas of reduced water column in ice shelf grounding zones. Comparing model estimates with our M4, MS4 and MN4 values shows that models do not accurately represent these terms.

1. Introduction

Accurate prediction of ocean tides around Antarctica is required for two fundamental reasons. First, ocean tides interact with the floating ice sheet [*Brunt et al.*, 2010b; *Doake et al.*, 2002; *Legresy et al.*, 2004; *Riedel et al.*, 1999], directly or indirectly affecting its mass balance and flow, and possibly also playing a role in iceberg formation. In the ice sheet grounding zone, tides modify back stresses of inflowing glaciers producing, in some cases, tidal modulation of ice flow well upstream of the grounding line [*Anandakrishnan and Alley*, 1997; *Anandakrishnan et al.*, 2003; *Bindschadler et al.*, 2003; *Gudmundsson*, 2006; 2007; *King et al.*, 2010; *Murray et al.*, 2007; *Riedel et al.*, 1999; *Thomas*, 2007]. The tidal contribution is not just periodic, but may include augmentation of the time-averaged flow rate [*Gudmundsson*, 2007; *King et al.*, 2010]. For example, *Gudmundsson* [2007] predicted that the time-averaged speed of Rutford Ice Stream, Antarctica, would be ~5% smaller in the absence of tides in the grounding zone.

Second, ocean tides represent a contaminating noise source in satellite and airborne geodetic measurements of ice velocity, elevation and mass change. Ocean tides bias estimates of ice velocity from single difference Interferometric SAR (InSAR). In ice elevation time series derived from the ERS satellite radar altimeter operating in its standard 35.00-day repeat interval orbit, tides can alias to large-amplitude signals with periods of several months to one year [*Andersen*, 1994], affecting measurements of seasonal surface elevation change of floating ice and ice shelf elevation from which ice thickness is estimated. Perhaps most significant for present studies of ice sheet mass changes, however, is the aliasing of tides in the Gravity Recovery and Climate Experiment (GRACE) satellite mission results. Aliasing periods for GRACE include 161 d (S2), 323 d (S1), 3.8 y (K2) and 7.7 y (K1) [e.g., *Moore and King*, 2008] and, at least for S2, the aliased signal amplitude is close to that of the unmodelled signal amplitude [*Melachroinos et al.*, 2009]. The S2 aliasing period is

sufficiently distinct from those of common geophysical processes to be estimated and removed [*Schrama et al.,* 2007], but the S1, K2 and K1 aliased periods are not easily separable from geophysical processes and hence will bias GRACE-derived estimates of Antarctic ice mass balance and glacial isostatic adjustment [*Riva et al.,* 2009]. Furthermore, through loading of the solid earth the ocean tides indirectly affect geodetic measurements of crustal motion from the Global Positioning System (GPS) [*Dach and Dietrich,* 2001; *King et al.,* 2005; *Thomas et al.,* 2008] and gravity change [*Agnew,* 1995; *Doi et al.,* 2009; *Knopoff et al.,* 1989; *Sato et al.,* 2001]. In the case of GPS, these can produce spurious signals at aliasing periods of several weeks to years [*King et al.,* 2008; *Penna et al.,* 2007; *Yuan et al.,* 2009] which could bias measurements of tectonics or glacial isostatic adjustment.

By subtracting the modeled best estimate of the tidal contribution from satellite-derived signals, most of the aliased tidal signal will be removed. For some regions around Antarctica, however, comparisons between in situ data and model results indicate that the ocean tide model error can be as much as 0.1 m for one or more tidal constituents [*Han et al.,* 2005; *King and Padman,* 2005; *King et al.,* 2005]. This is substantially above the error of tide models in the deep open ocean [*Fok et al.,* 2010]. Poor tide model performance in coastal zones is not unique to Antarctica; however, the presence of ice shelves and sometimes poorly defined coastlines and water column thicknesses complicates attempts to improve models [*Padman et al.,* 2002; *Ray,* 2008], and the paucity of high-quality, *in-situ* time series limits assessment of model errors and the ability to improve models through data assimilation.

Analysis of GRACE data has helped show that the largest errors in modern tide models applied to Antarctica, for the large-amplitude tidal constituents M2, S2 and O1, occur in the Weddell Sea region, particularly the portions beneath the large ice shelves [*Bosch et al.,* 2009; *Han et al.,* 2005; *Han et al.,* 2007; *Schrama et al.,* 2007]. An alternative GRACE data analysis approach has provided tidal estimates for K1 and P1 [*Han et al.,* 2010], which when

compared to modern tidal models again highlighted the poor accuracy of the models in the Weddell Sea region. However, because the spatial resolution of GRACE is several hundred km, GRACE can only provide a low resolution view of tide model performance for a limited set of tidal constituents, at least with the present record lengths. Sources of tidal data with higher spatial resolution include radar altimetry [*Fricker and Padman,* 2002; *Shepherd and Peacock,* 2003] and laser altimetry [*Padman et al.*, 2008; *Ray,* 2008], and GPS [*King and Padman,* 2005]. Radar altimetry is limited in accuracy for measuring tidal displacement and the ERS/Envisat orbit repeat period of 35.0 days prevents adequate sampling of certain tidal constituents, notably S2, K1 and P1. Laser altimetry is limited by surface effects and the relatively short record length, and works best at the highest latitudes where crossovers are closely spaced [*Padman and Fricker,* 2005; *Padman et al.*, 2008]. GPS is limited to the few records that have been collected on the Antarctic ice shelves to date [*King and Padman,* 2005], although it is the most accurate point-wise technique presently available for measuring the ocean tidal variability of an ice shelf's upper surface, at least without drilling through ice shelves to place bottom pressure recorders.

In this paper we describe a new and spatially extensive GPS-based tidal dataset for the two major Weddell Sea ice shelves – the Larsen C and Filchner-Ronne ice shelves (LCIS and FRIS, respectively). The records span several weeks to two years depending on location, and fill a major gap in the observation of tides around Antarctica. These represent independent data through which we validate recent global and regional ocean tide models for all major tidal constituents in this region. They also represent a new dataset which may be assimilated into models, although they are presently independent of the models we examine here. We also compare observed high-frequency, nonlinear tides with modeled ones where available. Our new data set only provides information on tide heights; however, improved knowledge of heights will also improve future modeling of tidal currents, which are important contributors

to ice shelf mass loss and sea-ice evolution [e.g., *Makinson and Nicholls*, 1999; *Makinson et al.*, 2011; *Padman and Kottmeier*, 2000].

2. Observations and Models

2.1 Data analysis strategy

GPS time series have been used to measure ocean tides on Antarctic ice shelves and sea ice since the 1990s [*Aoki et al.*, 2000; *Bondesan et al.*, 1994; *Riedel et al.*, 1999]. However, few records are available of sufficient length to allow separation of the major tidal constituents. The Antarctic Tide Gauge (ATG) Database (http://www.esr.org/antarctic_tg_index.html) [*King and Padman*, 2005] lists all known measurements for which data are publicly available. In November-December 2007, we deployed 10 geodetic GPS receivers on FRIS and three on LCIS. Three further records have since been obtained from LCIS plus an additional three records on FRIS near Evans Ice Stream as part of other projects. Details of the new GPS sites are listed in Table 1. Figure 1 shows the location of the new sites as well as the previous tidal records (GPS and other systems) in the ATG database: the new data significantly increase the spatial density of tidal records in this region.

Two sites on LCIS (SLGS and SLGN) are only a few km apart, so we use only the slightly longer SLGN record. Similarly, the Evans Ice Stream sites (EE2B, EE4B, EE55) are sufficiently close together to provide essentially the same tidal information and we only consider the longest of the records here (EE55). A fourth Evans site is partially grounded (EE4A) and we use it below only for investigation of nonlinear tides.

Four of the sites (FR05, FR07, FR09 and LAR2) were equipped with power systems designed to run through the winter and we obtained nearly complete annual time series for these. LAR2 was redeployed for a further year although due to snow accumulation it needed to be

raised, introducing a discontinuity in its time series. This site also experienced some melting in early 2008, producing a further offset that is easily seen in the horizontal coordinate time series. We manually corrected these offsets in the time series. We obtained high quality data from all sites, with record lengths spanning between 18 days and ~2 years (Table 1).

The present generation of tide models assumes that ice shelves are freely floating (hydrostatic) all the way inshore to the grounding line, even though there is a region of tidal flexure, several km wide, between the grounding line and the freely floating ice shelf [*Rignot et al.*, 2000]. Thus, any GPS sites within a few km of the grounding line should be excluded from direct comparisons with tide models. However, the grounding line around Antarctica is not always well defined, with uncertainties of tens of km being possible in certain locations (e.g., *Fricker and Padman* [2006] and *Brunt et al*. [2010a]). The estimate shown in Figure 1, based on feature analysis in the Mosaic of Antarctica (MOA) composite of MODIS satellite images [*Haran et al.*, 2005; *Scambos et al.*, 2007] suggests that several of our sites may be within the grounding zone or even inshore of the grounding line. For example, site EE2B is suggested to be on grounded ice, although it clearly shows a tidal signal not noticeably damped when compared to nearby sites EE4B and EE55, indicating that the grounding line position is in error by tens of kilometers: this is consistent with the recent InSAR analysis performed by *Sykes et al.* [2009]. Comparison of each site time series with nearby sites and model predictions suggests that all of the sites (apart from EE4A) are sufficiently distant from the ice shelf grounding line to be unaffected by grounding zone ice mechanics and therefore reflect sub-ice-shelf ocean tidal motion.

The GPS data were analyzed using a precise point positioning approach [*Zumberge et al.*, 1997], following the work of *King and Aoki* [2003], using GIPSY v5.0 [*Webb and Zumberge*, 1995] with homogeneously reprocessed satellite clocks and orbits from JPL. We modeled the solid earth tides according to IERS2003 conventions [*McCarthy and Petit*, 2004]. We also

modeled the ocean tide loading displacement based on the TPXO6.2 tide model [*Agnew*, 1997; *Egbert and Erofeeva*, 2002], one of the most accurate models for this region [*King and Padman*, 2005; *Thomas et al.*, 2008]. Any error in the ocean tide loading displacement introduced by the inaccuracy of the tide model is less than ~1 mm. Other pertinent GPS observation models include the VMF1 mapping function [*Boehm et al.*, 2006] and hydrostatic zenith delays derived from ECMWF [*Tregoning and Herring*, 2006]. Ambiguities were not fixed to integers, with only a small increase in coordinate time series noise. We produced coordinate time series with an interval of 5 min from which we extracted the height component for further examination here.

We removed from these series the effects of displacement of the solid earth due to atmospheric pressure loading, interpolating values obtained at 6 h time-steps [*van Dam et al.*, 1994] to the GPS data epochs. We did this in a reference frame compatible with the GPS time series over non-secular timescales (in the "centre of figure reference frame"; [see *Blewitt*, 2003]), and using an inverse barometer assumption and applying a low pass filter to remove signal with period <2 d where the inverted barometer assumption does not apply, as described below. For our stations the signal is typically within the range ±5 mm but occasionally approaches 15 mm.

2.2 Harmonic analysis

We determined tidal constituents for the ice shelf sites using the Matlab® t_tide toolbox [*Pawlowicz et al.*, 2002] based on the harmonic analysis methodology described by *Foreman* [1977]. For short records it is not possible to separate tidal constituents that are close in frequency using the data alone. For these records we used inference to separate the S2 and K2 semidiurnal components, and K1 and P1 diurnal components. The phase and amplitude

relationships used for inference were taken from nearby long records or from the CATS2008a tidal model (described later): see Table 1 for selection of inference parameters. At FR08 the harmonic analysis approach did not produce reliable results due to the brevity of its record, so we used a response method [*Cartwright and Ray*, 1990; *Groves and Reynolds*, 1975; *Munk and Cartwright*, 1966].

2.3 Inverse barometer effect

The de-tided time series are dominated by the atmospheric "inverse barometer effect" (IBE), and its presence may bias the estimated constituents, although this tends to be limited to the long period terms where most of the atmospheric energy lies. One exception is for very short records such as FR08. *Padman et al.* [2003] studied the IBE for Antarctic ice shelves and nearby oceans and found the relation between sea surface height (η_{IB}) and air surface pressure (P_{air}) was given by $\eta_{IB} \approx sP_{air}$, with s in the range -0.94 to -0.98 cm hPa^{-1}, a few percent less than is obtained under the assumption of isostasy (-1.01 cm hPa^{-1}). We repeated this analysis on our four longest records (FR05, FR07, FR09 and LAR2) after estimating and removing constituents with diurnal frequency and higher. The squared coherence of the GPS and pressure signals was >0.8 for signals with periods between about 2 d and 10 d, consistent with the "weather band" identified by *Padman et al.* [2003]. We then applied a band-pass (2-10 d) finite impulse filter to the datasets and computed a regression to obtain estimates of s for each site. For the FRIS sites the values of s were -0.884 (FR05), -0.862 (FR07), and -0.885 (FR09); for LAR2 on LCIS, s=-0.930 cm hPa^{-1}. The latter value is in close agreement with those determined for other ice shelves by *Padman et al.* [2003]; the FRIS values are substantially lower, and ~10% lower than expected from isostasy. However, they are close to

the value of ~-0.90 cm hPa^{-1} found for a similar band for the Ross Sea at coastal tide gauges close in McMurdo Sound, close to the front of the Ross Ice Shelf [*Goring and Pyne*, 2003].

GPS data analyzed by *Padman et al.* [2003] were not corrected for displacements of the solid earth due to atmospheric pressure loading , unlike in our analysis. Repeating our analysis without making this correction produced coefficients of -0.907 (FR05), -0.877 (FR07), -0.896 (FR09) and -0.940 cm hPa^{-1} (LAR2). The difference is systematic in that coefficients determined after removal of atmospheric pressure loading displacements are consistently lower. The mean difference is 0.015 cm hPa^{-1}, equivalent to 0.75 cm over a 50 hPa pressure change. Consequently, the *Padman et al.* [2003] coefficients for IBE are likely over-estimated by about this amount.

To correct the shorter tidal records we apply the IBE correction using the mean value for FRIS (0.877 hPa^{-1}) and the LAR2 value for all LCIS records. We then re-estimated the tidal constituents, with the final set given in Table S1 in supplementary material. Local pressure data were not available for some sites (Table 1) and so we did not apply the IBE correction; this has negligible effect on semi-diurnal and diurnal constituents, but it does impact the accuracy of other terms, particularly long period terms such as Mf and MSf.

2.4 Constituent accuracy and temporal stability

Tidal modulation of ice flow has been observed on the Rutford Ice Stream [*Gudmundsson*, 2007] and LCIS (M.A. King et al., Nonlinear interaction between ocean tides and the Larsen C Ice Shelf system, manuscript submitted to Geophysical Research Letters, December 2010). This modulation of speed invokes a horizontal strain within the ice shelf which reaches about $5x10^{-6}$ for the diurnal and semidiurnal frequencies. Assuming ice to be close to

incompressible at tidal periods [*Jenkins et al.*, 2006], the horizontal strain produces a vertical strain of the same magnitude. Over the thickness of the ice shelf (order 300 m), this results in a vertical tidal signal, not directly due to ocean tides, of up to ~1.5 mm in terms of ice shelf thickness or, after considering ice shelf buoyancy, <0.2 mm in ice shelf elevation as measured by GPS. The values for the signal at frequencies higher than twice per day are significantly smaller and hence negligible. Tidal variations in the thickness of FRIS have also been observed, with changes in ice shelf thickness as much as 35 mm [*Jenkins*, 2006], equivalent to ~4 mm of elevation change; the per-constituent bias is therefore <~1-2 mm.

Sub-daily GPS coordinate time series may be biased in some tidal bands by satellite orbit modeling errors or signal multipath [*King et al.*, 2008]. To confirm the accuracy of the GPS time series we performed two tests. First, we analyzed data from the nearby onshore International GNSS Service [*Dow et al.*, 2009] site PALM (Figure 1) in exactly the same way using the same time window as available for site LAR2. We found the only statistically significant errors related to S1 and K1 and their harmonics, and always with amplitude less than 3 mm. The only major tidal constituents affected are S1 (2.5 mm), K1 (1.6 mm) and K2 (2.6 mm). Second, we examined the agreement of closely spaced sites. Two sites (SLGN and SLGS) are located within 6 km of each other on Larsen C Ice Shelf (Figure 1) and their comparison provides an assessment of site-specific errors. Their independent tidal analysis gave constituents that agree to within 5 mm for the major constituents and hence are within the 95% confidence interval based on the t_tide analysis. These are relatively short records (Table 1) and uncertainties from longer records will be even smaller. Thus, we consider the analysis of the ice shelf GPS data to be free from substantial/significant systematic error.

In addition, we examined the reliability of the ice shelf constituent estimates by subdividing the longer records into 3-month sections. The amplitudes of the well-defined M2 and O1

constituents are stable to well within the uncertainty given by t_tide (~10-25 mm for 3-month record lengths).

Some signals from non-oceanographic effects are in the time series, such as surface snow densification; however, as with the inverse barometer effect, these do not occur at tidal periods and hence are only sources of time series noise. We consider other effects at tidal timescales, such as ice shelf inertia, to be negligible. The wavelengths and offshore decay length scales of tidal waves propagating under ice shelves are generally long compared with the flexure length-scale (<10 km) revealed by flexure near the grounding line [e.g., *Rignot et al*., 2000; *Fricker and Padman*, 2006]; therefore, we assume that the ice accurately conforms to the tidal deformation of the sea surface. Therefore, aside from the small tidal systematic errors quantified above, in what follows we take the measured surface motion of the ice shelf at tidal frequencies to be an accurate reflection of the motion of the ocean surface beneath it and hence that we are precisely measuring the amplitudes and phases of ocean tides.

3. Model comparison

3.1 Model information

We compare the tidal constituents computed above with model output from three recent global (FES2004, TPXO7.2 and GOT4.7) tide models and one regional (CATS2008a) model (see details in Table 2). Other models exist, but the four selected models are the most up to date at the time of writing. One notable exception from Table 2 is EOT08a [*Bosch et al.*, 2009]Athigh latitudes, EOT08a relaxes towards FES2004, its predecessor model, which is included here. Otherwise, the models are the same as, or updates of, those examined by Ray *et al.* [2009]. Of the models considered, TPXO7.2 is the only one to include GRACE data

assimilation [*Egbert et al.*, 2009]. CATS2008a is the only model to assimilate ice shelf altimetry, in the form of ICESat data [*Padman et al.*, 2008], as opposed to ocean altimetry. FES2004 is of particular interest as GRACE Release 4 analysis uses it globally to detide GRACE data; thus, any errors in tidal predictions from FES2004 have been aliased into GRACE time series.

Aside from the eight major tidal constituents, which are included in all models we consider, the inclusion of other tidal constituents varies between models (Table 2). Various nonlinear constituents are also included in all but CATS2008a in an attempt to capture nonlinear shallow water effects related to the generally dominant M2 constituent. Long-period terms (Mf=13.66 d, Mm=27.56 d, etc.) are also included in most models but we do not include them here, as our new records are generally too short to examine them robustly. Instead, we focus below on semi-diurnal, diurnal and nonlinear terms.

The models are provided on regular grids of varying resolution (Table 2) and hence must be interpolated to the actual site location. We do this based on modified versions of the software supplied with each tide model. To allow for minor variations in the model domains, we needed to move up to two sites in each model up to a few tens of km in order to obtain a prediction. The two sites in the inlet close to Rutford Ice Stream are well outside GOT4.7's model domain, and there the model values were set to zero to represents the error introduced into altimetry, or GRACE, if this model was used for de-tiding.

3.2 Misfit

When comparing observations and models we compute a model misfit, regarding the observations as being error-free. We computed the root-mean-square (RMS) error σ_k for a

given constituent *k* and the root-sum-square (*RSS*) error for the combination of the eight major constituents (σ_C) as follows:

$$\sigma_k = \sqrt{\frac{1}{2N}\sum_{j=1}^{N}\left|Z_j^m - Z_j^o\right|^2} \quad (1)$$

and

$$RSS = \sqrt{\sum_{k=1}^{8}\sigma_k^2} \quad (2)$$

where *N* is the total number of locations, and $Z_j = H\left[\cos(G) + i\sin(G)\right]$ is the complex expression of the interpolated modeled (*m*) and observed (*o*) tide amplitudes (*H*) and Greenwich phases (*G*) respectively for the relevant constituent at site *j*.

To increase spatial coverage of the Weddell Sea, we supplement the new sites given in Table 1 with additional pre-existing records from *King and Padman* [2005], mostly from outside the ice shelves (Figure 1). Some of these additional records have been assimilated into some of the tide models, which will artificially reduce the misfit.

4. Model accuracy

4.1 Major diurnal and semi-diurnal terms

The misfit magnitude for each site, $\left|Z_j^m - Z_j^o\right|$, is shown in Figures 2-6 for M2, S2, K1, O1 and K2 respectively. Figures for the other major terms are provided in the supplementary material (Figures S1-3). The misfit statistics (Eq. 1 and 2) are given in Table 3. All models experience problems at some sites which tend to inflate σ_k and *RSS*; so we removed,

somewhat arbitrarily, the two least accurately modeled sites for each model and recomputed the statistics (Table 4). These sites are shown in Figures 2-6. We do not discriminate between short and long records apart from the use of different symbols in Figures 2-6. We show below that any difference in observational accuracy is less than the model misfits.

Considering M2, Table 3 shows σ_{M2} is either 7-8 cm (TPXO7.2 and CATS2008a) or >25 cm (GOT4.7 and FES2004). After removing the two least accurate sites in each model, this reduces to 4.8-8.0 cm for all models (Table 4), although FES2004 and GOT4.7 remain the least accurate overall. All models have large misfit magnitudes (>25 cm) for at least one site (Figure 2). Large misfit at the site near Doake Ice Rumples (labelled as DIR in Figure 1) is common to all models with misfit vectors having amplitudes of 40-50 cm. Closer examination suggests that the modelled phases are offset from the observed by about 20°. This record of vertical displacement was obtained through applying an elastic beam model to tiltmeter data [*Smith*, 1991]. The elastic beam model may be a source of error as more rigorous viscoelastic modelling of ice tidal tilt is now known to produce phase differences compared with pure elastic modeling [*Reeh et al.*, 2003]. However, we note that another tiltmeter record at Rutford Ice Stream (RIS, Figure 1) is in close agreement with a GPS record there. All but CATS2008a exhibit poor agreement with the sites near the grounding line of Rutford Ice Stream, but this is related to the respective model domains and differences in which nearby records were assimilated.

GOT4.7 is relatively inaccurate for LCIS, with misfit magnitudes reaching 25 cm, although no models have consistent σ_{M2} below 5 cm there. FES2004 exhibits an east-west divide in its misfit magnitudes, with high values in LCIS and the western FRIS. Assimilation of GRACE data into TPXO7.2 has not increased the model accuracy at M2 markedly relative to other

models, which is in agreement with the more limited Weddell Sea tide gauge comparison of *Egbert et al.* [2009].

Figure 3 illustrates that S2 has marginally lower σ_k than M2, with values of 4-5 cm (Table 4). The misfit magnitudes in the eastern Weddell Sea, away from the ice shelves, are small in all models, although still typically above the σ_k seen in the deep ocean (2-3 cm). All models except TPXO7.2 show significant misfit for LCIS, with errors increasing toward the western grounding zone. The reduced error in TPXO7.2 in LCIS compared with other models is likely partly due to the GRACE data assimilation; although we note that substantial error in the western FRIS persists.

Greater between-model differences are seen in the major diurnal constituents. In both O1 and K1 (Figures 4-5), CATS2008a is in particularly good agreement with LCIS observations, whereas the other models show large misfit magnitudes; for GOT4.7, the O1 misfit magnitudes approach or exceed 25 cm. The GOT4.7 amplitudes of O1 and K1 under the LCIS are too large by about 17 and 10 cm, respectively, with some phase error as well. A large residual is not evident in the GRACE estimates of *Han et al.* [2010], where errors of only a few cm are evident in GOT4.7. This difference is presumably due to the spatial resolution limitations of GRACE. For the larger region of FRIS, however, our results are in overall agreement with the estimates of *Han et al.* [2010], who showed 5-6 cm errors in K1 for GOT4.7. Overall, CATS2008a with σ_k (Table 4) of 1.7 cm (O1) and 2.9 cm (K1) has 10-40% lower misfit than the other models. These misfits approach the levels of misfit seen at deep ocean sites, but improvements can also be made, especially in K1 for the FRIS domain.

K2 errors are substantially smaller than the other semidiurnal terms (Figure 6), with σ_{K2} below 2 cm (Table 4). FES2004 and TPXO7.2 do show, however, a band of increased misfit along the southern FRIS grounding zone. The small σ_{K2} is typical of the σ_k for P1, Q1 and N2

(see Figures S1-3 in supplementary material), although inter-model and inter-region variations exist. P1 in all models is in noticeably worse agreement in LCIS when compared to FRIS, but still generally less than ~5 cm. *Han et al.* [2010] show GRACE-derived residuals with respect to GOT4.7 for P1, with ~2-3 cm signal over the front of FRIS. We do not observe an increase of misfit magnitudes at the FRIS ice front. We therefore assume the observation of tide error under FRIS by *Han et al.* [2010] must be a GRACE resolution effect and tide modeling error is confined to the region immediately seaward of the ice shelf front. For N2 misfit, LCIS stands out as having consistently larger misfit than other regions. Of the four models, TPXO7.2 shows the smallest errors there, although on FRIS they are slightly larger than the other models. Likewise, LCIS has the largest misfit magnitudes for Q1, with CATS2008a being worst. Overall, though, tide model prediction error for P1, Q1 and N2 are small and σ_k is $\leq$2 cm per constituent for all models. Considering the small errors, aliasing of mismodeled K2, N2, P1 and Q1 tides into GRACE time series should be small in this region.

Considering together all 8 major tidal constituents, the misfit *RSS* (eq. 2) suggests that CATS2008a is in closest agreement with the observations (Tables 3 and 4), with TPXO7.2 only marginally less accurate. However, as we have discussed, the agreement is highly dependent on the actual tidal constituent, and no one model is most accurate for the entire region or for all constituents. This is in agreement with conclusions from a recent global study [*Ray et al.*, 2009]. When examining signal at the 161-d S2 alias period in GRACE it is critical, therefore, that the S2 error magnitude is not assumed to be similar to the accuracy of other tidal constituents. We conclude that there is an ongoing need for improvement in model prediction accuracy in this region, especially for the most energetic constituents.

The difference between FES2004 and CATS2008a is shown as background shading in Figures 2-5. Comparison with actual misfits of each of the models suggests that model

differencing in this region may substantially misrepresent the error, and sometimes underestimate it. This suggests that some of the models are correlated with each other, possibly due to some common setup error(s). This has implications for simulation studies that rely on tide model differencing to examine potential effects on GRACE [*Moore and King*, 2008; *Ray et al.*, 2001; *Seo et al.*, 2008].

4.2 S1 tide

S1 tides alias into GRACE mass change time series at approximately seasonal timescales [e.g., *Moore and King*, 2008] and may therefore bias seasonal ice mass change estimates. S1 has its origin mainly in radiational rather than gravitational forcing. At high latitudes, the forcing magnitude of S1 is small as a result [*Pedley et al.*, 1986]. We can separate it from K1 at four sites and the estimated amplitudes and phases are given in Table 5. Considering the magnitude of the potential GPS systematic error (see PALM, Table 5), the signal at FR09 is too small to consider further. Sites FR05 and FR07 show better signal to noise ratio (~2), while the most robust signal is at LAR2. Modeled S1 estimates are provided by GOT4.7 and FES2004. In the case of GOT4.7 these have been set to zero in polar seas and hence we do not consider this further here. For LAR2, FES2004 amplitude is about 50% of the observed signal, with close agreement in phase. The amplitude is in closer agreement at FR05 and FR07, although with larger phase differences, particularly for FR07.

Ray et al. [2009] reported S1-related GRACE anomalies, showing a small anomaly at the location of LCIS (their Figure 11a) while no anomaly is evident for FRIS. Since they detided with GOT4.7, in which has S1 is set to zero amplitude at high latitudes, these anomalies reflect the influence of the total S1 tides on GRACE. These observations provide, therefore, some corroboration of our observation of significant S1 under the LCIS.

4.3 Nonlinear tides

In this section we consider signals with frequency higher than 2 cycles per day (cpd). Most signals in these frequency bands tends to have their origin in nonlinear interactions of the diurnal and semidiurnal tidal species, with the resulting frequencies being close to integer cycles per day. These interactions are most commonly due to shallow water effects and hence are most prominent on continental shelves [*Le Provost*, 1991; *Pugh*, 1987]. Nonlinear tides have previously been observed under Antarctic ice shelves [*Capra et al.*, 1999; *Eckstaller and Miller*, 1984; 1985; *Lutjeharms and Stavropoulos*, 1985; *Pedley et al.*, 1986; *Potter et al.*, 1985; *Smith*, 1991] and nearby seas [*Goring and Pyne*, 2003]. *Eckstaller and Miller* [1984; 1985] reported on tidal gravity observations of nonlinear tides for a site near to our FR09 site, but not at two sites further north, including one near our FR10 site. *Pedley et al.* [1986] suggested that some nonlinear tides may be excited by a nonlinear response of the ice shelf to ocean tide forcing. In particular they speculated that an anelastic component in the deformation of ice in ice shelf grounding zones may produce these effects. Later, we briefly discuss possible oceanographic and glaciological origins of this signal.

Spectra for a selection of our GPS sites (Figure 7) show significant energy near 3, 4, 5 and 6 cpd, and a small peak at 7 cpd. FR07 shows some reduced power at 4 cpd compared with the other sites, but otherwise the sites are in close agreement. These high frequency signals suggest the presence of nonlinear tides under the ice shelf. In general, the spectra are similar to those near George VI Ice Shelf [*Pedley et al.*, 1986], near Doake Ice Rumples on FRIS [Figure 1, *Smith*, 1991], and at coastal tide gauges near the front of Ross Ice Shelf [*Goring and Pyne*, 2003]. At our sites the power at 3 cpd, relative to the other bands, is lower than shown by *Pedley et al.* [1986] and more akin to that shown by *Smith* [1991]. The Ross Ice

Shelf record did not show power at 5 or 6 cpd; however, we note that this was not a sub-ice-shelf record.

The interpretation of these records is complicated by systematic error in GPS coordinate time series, especially those relating to K1, K2 and S2 [*King et al.*, 2008]. However, the spectrum of the PALM record (Figure 7 bottom) suggests that these are limited to discrete frequencies very close to integer cycles per day. Tidal analysis reveals these near-integer peaks are limited to combinations of S2, K2 and K1 such as SK3, S4 and 2SK5. Therefore, we limit our discussion here to signal at other frequencies.

We modified our tidal analyses to include estimating several common nonlinear terms alongside those at semidiurnal, diurnal and longer periods. We found signal with amplitude greater than ~1 cm at a number of frequencies and show these in Figure 8. The μ_2 harmonic is not a nonlinear term, but its frequency is coincident with the nonlinear 2MS2 and so we include it here and discuss it further below.

No nonlinear term exceeds 3 cm in amplitude and all have substantial spatial variation. The largest amplitudes are found for M4, SP3 and MO3. In terms of spatial pattern, inter-constituent cross-correlations are weak. For instance, M3 has largest amplitude on LCIS and in the south-west FRIS, while MO3 has small amplitude on LCIS and larger values around the grounding zone of FRIS. 2MS6 is also small at LAR2, but larger near Evans Ice Stream and FR09.

Of particular interest are M4, MS4 and MN4 as these are now included in some tide models: TPXO7.2 includes these three terms, while FES2004 and GOT4.7 include M4. We tabulate the results from our analysis alongside the modeled values in Table 7.

Considering M4, the TPXO7.2 amplitudes are significantly smaller than observed. Observed amplitudes range from 0.4 to 2.6 cm, while the modeled values do not exceed 0.9 cm. Both FES2004 and TPXO7.2 generally underestimate M4 amplitudes, although they are larger in FES2004. The exception is for the Evans Ice Stream sites, where they are overestimated. The phases are in poor agreement everywhere. GOT4.7 contains non-zero M4 amplitudes for LCIS only, but these were included in GOT4.7 in error and are not intended for interpretation (Richard Ray, pers. comm., October 2010).

In contrast to M4, MS4 values tend to be too large in TPXO7.2, often substantially so. As with M4, phase discrepancies are also large. For MN4, TPXO7.2 amplitudes are too small, as with M4; however, the phases are generally in much closer agreement with the observations. The nonlinear terms included in the TPXO7.2, FES2004 and GOT4.7 models usually agree poorly with the observations. They must, therefore, be regarded as unreliable in this region and the models may benefit from assimilation of the tidal coefficients obtained from our new GPS records and from reanalysis of older GPS and tide gauge records in the ATG database [e.g., *Egbert et al.*, 2010].

Several other authors have considered nonlinear tides in Antarctica and show spectra, but the amplitudes and phases are not always tabulated. Results have been reported for Fimbul Ice Shelf and offshore of Ekström Ice Shelf [*Lutjeharms and Stavropoulos*, 1985] and in Terra Nova Bay [*Capra et al.*, 1999]. In each case the amplitudes are no larger than 1.0 cm, so the values we obtained from LCIS and FRIS are high in comparison. These amplitudes are not large when considering other continental shelf areas globally, however, and both LCIS and FRIS experience much larger fundamental tides (diurnal and semidiurnal) than for these previously analyzed ice shelves. *Andersen* [2004] reported on the northwest European shelf and showed M4 and MS4 amplitudes approaching 20 cm and 5 cm, respectively. *Glorioso and Flather* [1997] showed M4 and MN4 amplitudes for the Patagonian Shelf reaching 15

and 8 cm respectively. Both regions, therefore, have amplitudes substantially larger than we show here. Nevertheless, the nonlinear tides under LCIS and FRIS are not negligible and may, indeed, provide clues to further improvements in tide model parameterization [see *Egbert et al.*, 2010; *Le Provost*, 1991].

Using a limited dataset, *Pedley et al.* [1986] observed that nonlinear tides at 3 cpd are smallest at the ice shelf fronts and increase with distance under the ice shelves. The spatial pattern of MO3 (Figure 8) is in agreement with this, but M3 and SP3 show more complex spatial patterns. If the observation of *Pedley et al.* [1986] were a general principle, then the power at 3 cpd for FR05 and FR09 should be significantly greater than for FR07; however, they are not (Figure 7).

The conventional treatment of nonlinear tides assumes that they originate in shallow seas, mainly due to the effects of bottom friction. In ice-shelf regions the frictional effects are further increased by friction at the ice shelf base. However, it is also possible that horizontal glaciological forcing contributes to these signals. *Pedley et al.* [1986] also noted the potential for a horizontal glaciological forcing, but restricted it to signal at 4 cpd. It is now known that there are high frequency (>2 cpd) variations in ice flux across the grounding line of Rutford Ice Stream [*Murray et al.*, 2007], caused by a nonlinear response to vertical tidal forcing in its grounding zone [*Gudmundsson*, 2006; 2007; *King et al.*, 2010]. The effect of this "pumping" on measured FRIS ice shelf displacement at tidal periods is yet to be explored. A theoretical study predicted Rutford Ice Stream velocity variations in the 3, 4 and 6 cpd bands [*King et al.*, 2010]. Observations appear to confirm the presence of signal in these bands, although the most significant signal is at 5 cpd [*Murray et al.*, 2007]. GPS measurement errors may contribute to the observed signal [e.g., *King et al.*, 2008]. We note that a similar nonlinear response to tidal forcing has been inferred for the glaciers flowing into LCIS (M.A. King et al., Nonlinear interaction between ocean tides and the Larsen C Ice Shelf system,

manuscript submitted to Geophysical Research Letters, December 2010). Apart from this, however, it is not known if the other ice streams and glaciers in this region respond to tides in their grounding zones in the same way. The expected non-linear tidal forcing from this glaciological mechanism is, therefore, not yet well defined and needs further study.

Our dataset does not allow us to distinguish between oceanographic and glaciological mechanisms for nonlinear tides on ice shelves. However, the sites near the grounding line of Evans Ice Stream are useful in examining the effect of water column thickness variation in ice shelf grounding zones as the signal at one site (EE4A) is within the grounding zone, with nearby sites freely floating. We presume that any pumping effect, if it exists, is similar at all sites. Considering the 1-2 cpd bands, the spectrum of tidal motion for EE4A is damped when compared with spectra for nearby sites (see Figure 7 middle). Constituent phases are largely unaffected by the damping. Comparing the power at higher frequencies suggests that there is an increase at 4 cpd relative to the other sites, but that power at 3 and 6 cpd is distinctly lower, with some reduction also at 5 cpd. This is consistent with the observation of *Pedley et al.* [1986] and *Eckstaller and Miller* [1984; 1985], who noted an apparent amplification at 4 cpd under the ice shelf; however, in the data set shown by *Smith* [1991], the signal at 4 cpd is not large relative to the other terms. In our datasets the increase in tidal amplitude is particularly notable at MS4 (300% larger at EE4A than at EE4B), with decreases at MO3 (55% smaller) and 2MS6 (85% smaller). Phase changes relative to the nearby sites are also evident (Table 2). This suggests that only a subset of our observed nonlinear tides is generated by grounding zone effects (i.e., those at 4 cpd) and that, if nonlinear tides are being excited by the presence of the ice shelf, then it must involve a further mechanism.

4.4 2MS2 and μ_2

Ray et al. [2009] showed GRACE range acceleration anomalies related to the frequency of μ_2 and noted that they predominate in shallow water seas. The μ_2 tide has a direct gravitational origin, but it shares the same frequency as the nonlinear 2MS2. Noting the presence of these anomalies in shallow water seas, *Ray et al.* [2009] suggested that they may relate to 2MS2 rather than μ_2. This has important implications for inference of minor tidal constituents, such as μ_2, in shallow waters.

The western boundary of the Weddell Sea is the only location in Antarctica where the GRACE μ_2 anomalies are evident [*Ray et al.*, 2009]. The spatial distribution of our dataset therefore allows us to examine this suggestion more carefully. We computed the amplitude ratio between M2 and μ_2 for the seven sites shown in Figure 8. The equilibrium tide amplitude ratio is 0.031 [*Pugh*, 1987]. Our computed values were all less than 0.020, with the exception of FR07 which had a value of 0.043, with negligible formal error. This suggests that μ_2 is not anomalously large. An alternative interpretation is that μ_2 is being partially cancelled by 2MS2.

We then compared the determined ratios to the GRACE range acceleration anomalies of *Ray et al.* [2009] using values we interpolated to the same locations. Based on the data (see their Figure 11), we took the background GRACE range acceleration noise level to be 0.20 nm s^{-2}. Using this, we found that the only significant GRACE anomaly for our site locations existed at FR07 with an anomaly of 0.31 nm s^{-2}. This correspondence of large anomaly with large observed amplitude ratio gives some weight to the suggestion of *Ray et al.* [2009] that the presence of GRACE anomalies in shallow water seas could be due to the presence of substantial nonlinear 2MS2. If this is the case, then *Ray et al.* [2009] suggest that methods used to infer minor tides in shallow seas need to be reexamined. We urge caution, however,

as our sample is very limited. We also note that one of the other large GRACE anomalies in this region is located onshore of the southern Antarctic Peninsula, and hence the dataset is not artifact free.

5. Discussion and Conclusions

We have introduced new and spatially extensive tidal measurements on the Larsen C and Filchner-Ronne Ice Shelves (LCIS and FRIS, respectively) in the Weddell Sea. We combined these with existing datasets and tested a range of modern global and regional tide models. Present-day state-of-the-art tide models commonly have *RSS* errors of 10-40 cm in the Weddell Sea, although excluding the worst two sites (from a total of 31) for each model reduced this to 7-12 cm. Tides under LCIS are particularly poorly modeled, with observation-model vector differences reaching 25 cm for some constituents. We hypothesize that these errors are due mainly to inaccurate water column thicknesses under LCIS due to a lack of water column thickness data; however, errors in modeled dissipation of tides through friction and anelastic deformation of ice may explain some of the model-data misfit. Differences of ~10 cm are common across large regions of FRIS. Single-constituent errors are largest (~4-8 cm RMS; Table 4) for the most energetic tides M2 and S2, reducing to ~1-7 cm RMS for O1 and K1. The errors are much reduced away from ice shelves and approach tide model accuracy for the global deep oceans. However, many of the open-ocean tide records, especially those along the eastern Weddell Sea coast east of Filchner Ice Shelf, have previously been included in some of the models (TPXO7.2, CATS2008a) through data assimilation; thus, the better model performance in these areas at least partially reflects the effects of assimilation.

A number of other factors may also affect the variation in tide model accuracy, including the accuracy of model geometry, the model resolution, the quality of open boundary conditions (for the sole regional model, CATS2008a), and the sophistication of the model physics. The latter includes whether friction is parameterized as linear or quadratic; whether any parameterization of energy transfer from the barotropic to baroclinic tide is included; and whether tides are modeled one constituent at a time or concurrently, allowing nonlinear interactions between constituents through advection and/or friction.

No single tide model is most accurate for all regions within the Weddell Sea and for all tidal constituents. This is in agreement with the global study of *Ray et al.* [2009]. However, considering the importance of K1 for GRACE data analysis, with a ~7 year aliasing period, using CATS2008a in GRACE analysis will deliver the most accurate results. For global GRACE data analysis this model will need to be supplemented by a global tide model; CATS2008a is forced at its northern boundary by TPXO7.1, an earlier version of TPXO7.2. Likewise, tidal aliasing into satellite altimetry measurements of LCIS elevation change will be minimized using CATS2008a, but not totally removed. Residual tides of ~5 cm will remain and affect GRACE and altimetry solutions until tide model error can be reduced further.

Importantly, FES2004, used in GRACE Release 4 products, has regional errors ~75% greater than CATS2008a for K1 and ~50% for all other constituents. This will bias GRACE solutions of ice mass change in this region, and in particular in the northern Antarctic Peninsula near LCIS. It is not clear to what extent the small spatial scale of LCIS mitigates this effect. The potential GRACE tidal aliasing effect was simulated by *Moore and King* [2008] who used the difference between TPXO6.2, an earlier version of TPXO7.2, and FES2004 as their tidal “error”. Comparing their Figure 2 with our Figure 5 suggests that these

differences generally overstated the tide modeling error except for LCIS where it was representative of the true error in FES2004.

Our comparison of ice shelf elevation changes with atmospheric pressure variations revealed strong coherence at periods of 2-10 d but with a response ~10% below that predicted by isostasy. However, these values for the inverse barometer effect are comparable to other studies using ice-shelf GPS data from elsewhere in Antarctica. We note that the two large ice shelves, the FRIS studied here and Ross Ice Shelf studied by *Goring and Pyne* [2003], exhibit particularly low values of the IBE (-0.88 to -0.90 cm hPa^{-1}, 10-12% below isostasy), whereas the smaller ice shelves where we have long records (Brunt and Larsen C) exhibit larger values (~-0.93 cm hPa^{-1}). We hypothesize that this difference in response arises from the different relationship between the atmospheric pressure and the wind stress in the presence of the "rigid" lid imposed by the ice shelf. Alternatively, larger shelves may be more difficult than small shelves to "flush" at short time scales, so that the ice shelf filters out the IBE response to high-frequency variability in P_{air}. Since the difference between the isostatic ("ideal") and measured IBE for these shelves can be a few cm, further work is required to understand how the ice shelf geometry influences IBE.

We identified tidal power at frequencies of 3-6 cpd in agreement with studies for other locations in Antarctica [e.g., *Lutjeharms and Stavropoulos,* 1985; *Pedley et al.,* 1986]. The amplitudes of these signals are substantially greater than has been previously reported in Antarctica. While three of the tide models we studied include one or more of the major nonlinear quarter-diurnal tides M4, MN4 and MS4, the models perform poorly in comparisons with our new data. We observed that nonlinear tides did not increase uniformly in amplitude at the one available grounding zone site compared to nearby sites outside the grounding zone. Instead harmonics at 3, 5 and 6 cpd decreased in amplitude while only the 4 cpd term increased. This suggests, therefore, that nonlinear tides are not all being generated

in these regions as was suggested previously by *Pedley et al.* [1986]. This is in agreement with their presence throughout both FRIS and LCIS. From our data we cannot determine whether the nonlinear tides originate through nonlinear oceanic processes such as friction (at the seabed and the ice base) or through a glaciological mechanism that might, for example, be related to the nonlinear response of ice stream discharge to vertical tidal forcing near the grounding line. Given that the total nonlinear tide signal can be large, up to several cm, resolving and modeling the source and spatial distribution of these tidal signals is important for improved tide removal from satellite and airborne geophysical data.

The new tidal constituents are included in an updated Antarctic Tide Gauge Database (http://www.esr.org/antarctic_tg_index.html).

Acknowledgements

The data collection and research were enabled by NERC (UK) Antarctic Funding Initiative grants to MAK/PJC, AS and BK. MAK was also funded by NERC and RCUK Academic Fellowships. LP was funded by NASA, NNX06AH39G and NNX10AG19G. We thank David Barber for his efforts in deploying the GPS units and BAS personnel based at Rothera for their additional and substantial efforts in maintaining the equipment and retrieving the data. We thank model authors for making their model output available. Richard Ray kindly provided GRACE range acceleration anomalies for μ_2 and commented on a section of a draft of the manuscript. We also thank JPL for making GIPSY and their orbit products available and Tonie van Dam for providing atmospheric pressure loading displacements. We gratefully acknowledge the efforts of two anonymous reviewers and the Editor. This is ESR contribution 138.

References

Agnew, D. C. (1995), Ocean-load tides at the South Pole - a validation of recent ocean-tide models, *Geophys. Res. Lett.*, *22*(22), 3063-3066.

Agnew, D. C. (1997), NLOADF: A program for computing ocean-tide loading, *J. Geophys. Res.*, *102*(B3), 5109-5110.

Anandakrishnan, S., and R. B. Alley (1997), Tidal forcing of basal seismicity of ice stream C, West Antarctica, observed far inland, *J. Geophys. Res.*, *102*(B7), 15183-15196.

Anandakrishnan, S., D. E. Voigt, R. B. Alley, and M. A. King (2003), Ice stream D flow speed is strongly modulated by the tide beneath the Ross Ice Shelf, *Geophys. Res. Lett.*, *30*(7), 1361, doi:1310.1029/2002GL016329.

Andersen, O. B. (1994), Ocean tides in the northern North Atlantic and adjacent seas from ERS 1 altimetry, *J. Geophys. Res.*, *99*(C11), 22557-22573.

Andersen, O. B. (2004), The M4 shallow water tidal constituent from altimetry and tide gauges, in *Satellite altimetry for geodesy, geophysics and oceanography*, edited by C. Hwang, et al., pp. 231-235, Springer-Verlag, Berlin.

Aoki, S., T. Ozawa, K. Doi, and K. Shibuya (2000), GPS observation of the sea level variation in Lutzow-Holm Bay, Antarctica, *Geophys. Res. Lett.*, *27*(15), 2285-2288.

Bindschadler, R., M. A. King, R. B. Alley, S. Anandakrishnan, and L. Padman (2003), Tidally Controlled Stick-Slip Discharge of a West Antarctic Ice Stream, *Science*, *301*(5636), 1087-1089.

Blewitt, G. (2003), Self-consistency in reference frames, geocenter definition, and surface loading of the solid Earth, *J. Geophys. Res.*, *108*(B2), 2103, doi:2110.1029/2002JB002082.

Boehm, J., B. Werl, and H. Schuh (2006), Troposphere mapping functions for GPS and very long baseline interferometry from European Centre for Medium-Range Weather Forecasts operational analysis data, *J. Geophys. Res.*, *111*, B02406, doi:02410.01029/02005JB003629.

Bondesan, A., A. Capra, A. Gubellini, and J. Tison (1994), On the use of static GPS measurements to record the tidal response of a small Antarctic ice shelf (Hells Gate Ice Shelf, Victoria Land), *Geografia Fisica Dinamica Quaternaria*, *17*, 123-129.

Bosch, W., R. Savcenko, F. Flechtner, C. Dahle, T. Mayer-Gurr, D. Stammer, E. Taguchi, and K. H. Ilk (2009), Residual ocean tide signals from satellite altimetry, GRACE gravity fields, and hydrodynamic modelling, *Geophysical Journal International*, *178*(3), 1185-1192.

Brunt, K. M., H. A. Fricker, L. Padman, T. A. Scambos, and S. O'Neel (2010a), Mapping the grounding zone of the Ross Ice Shelf, Antarctica, using ICESat laser altimetry, *Ann. Glac.*, *51*(55), 71-79, DOI: 10.3189/172756410791392790.

Brunt, K. M., M. A. King, H. A. Fricker, and D. R. MacAyeal (2010b), Flow of the Ross Ice Shelf, Antarctica, is modulated by the ocean tide, *J. Glac.*, *56*(195), 157-161, doi:110.3189/002214310791190875.

Capra, A., S. Gandolfi, L. Vittuari, C. Lusetti, and C. Stocchino (1999), Kinematic GPS for the study of tidal undulation of floating ice tongue, *Bollettino di Geodesia e Scienze Affini*, *LVIII*(2), 151-173.

Cartwright, D. E., and R. D. Ray (1990), Oceanic tides from Geosat altimetry, *J. Geophys. Res.*, *95*(C3), 3069-3090.

Dach, R., and R. Dietrich (2001), The ocean loading effect in GPS analysis: A case study in the Antarctic Peninsula region, *Mar. Geod.*, *24*, 13-25.

Doake, C. S. M., H. F. J. Corr, K. W. Nicholls, A. Gaffikin, A. Jenkins, W. I. Bertiger, and M. A. King (2002), Tide-induced lateral movement of Brunt Ice Shelf, Antarctica, *Geophys. Res. Lett.*, *29*(8), doi: 10.1029/2001GL014606.

Doi, K., K. Shibuya, A. Wendt, R. Dietrich, and M. A. King (2009), Tidal gravity variations revisited at Vostok Station, Antarctica, *Polar Science*, *3*(1), 1-12.

Dow, J. M., R. E. Neilan, and C. Rizos (2009), The International GNSS Service in a changing landscape of Global Navigation Satellite Systems, *J. Geodesy*, *83*, 191-198, DOI: 110.1007/s00190-00008-00300-00193

Eckstaller, A., and H. Miller (1984), Gezeiten-Vertikalbewegung des Filchner Schefeises (Tides and vertical movement of the Filchner Ice Shelf), *Berichte zur Polarforschung*, *19*, 82-97.

Eckstaller, A., and H. Miller (1985), Gravity tides on the Filchner Ice Shelf, paper presented at Filchner Ronne Ice Shelf Programme, Alfred Wegener Institute for Polar Research, Bremerhaven, Federal Republic of Germany.

Egbert, G. D., and S. Y. Erofeeva (2002), Efficient inverse modeling of barotropic ocean tides, *J. Atmos. Ocean. Technol.*, *19*(2), 183-204, doi:110.1175/1520-0426(2002)1019<0183:EIMOBO>1172.1170.CO;1172.

Egbert, G. D., S. Y. Erofeeva, S. C. Han, S. B. Luthcke, and R. D. Ray (2009), Assimilation of GRACE tide solutions into a numerical hydrodynamic inverse model, *Geophys. Res. Lett.*, *36*.

Egbert, G. D., S. Y. Erofeeva, and R. D. Ray (2010), Assimilation of altimetry data for nonlinear shallow-water tides: Quarter-diurnal tides of the Northwest European Shelf, *Continental Shelf Research*, *30*(6), 668-679, doi: DOI: 610.1016/j.csr.2009.1010.1011.

Fok, H. S., H. B. Iz, C. K. Shum, Y. Yi, O. Andersen, A. Braun, Y. Chao, G. Han, C. Y. Kuo, K. Matsumoto, and Y. T. Song (2010), Evaluation of Ocean Tide Models Used for Jason-2 Altimetry Corrections, *Mar. Geod.*, *33*(1 supp 1), 285 - 303.

Foreman, M. G. G. (1977), Manual for tidal heights analysis and prediction, Pacific Marine Science Report, 58 pp, Institute of Ocean Sciences, Sidney, B.C., Canada.

Fricker, H. A., and L. Padman (2002), Tides on Filchner-Ronne Ice Shelf from ERS radar altimetry, *Geophys. Res. Lett.*, *29*(12), 1622, doi:1610.1029/2001GL014175.

Fricker, H. A., and L. Padman (2006), Ice shelf grounding zone structure from ICESat laser altimetry, *Geophys. Res. Lett.*, *33*(15).

Glorioso, P. D., and R. A. Flather (1997), The Patagonian Shelf tides, *Prog. Oceanogr.*, *40*(1-4), 263-283.

Goring, D. G., and A. Pyne (2003), Observations of sea-level variability in Ross Sea, Antarctica, *New Zealand Journal of Marine and Freshwater Research*, *37*(2), 241-249.

Groves, G. W., and R. W. Reynolds (1975), An orthogonalized Convolution Method of Tide Prediction, *J. Geophys. Res.*, *80*(30), 4131-4138.

Gudmundsson, G. H. (2006), Fortnightly variations in the flow velocity of Rutford Ice Stream, West Antarctica, *Nature*, *444*(7122), 1063-1064.

Gudmundsson, G. H. (2007), Tides and the flow of Rutford ice stream, west Antarctica, *Journal of Geophysical Research-Earth Surface*, *112*.

Han, S.-C., R. Ray, and S. Luthcke (2010), One centimeter-level observations of diurnal ocean tides from global monthly mean time-variable gravity fields, *J. Geodesy*, 1-15.

Han, S. C., C. K. Shum, and K. Matsumoto (2005), GRACE observations of M-2 and S-2 ocean tides underneath the Filchner-Ronne and Larsen ice shelves, Antarctica, *Geophys. Res. Lett.*, *32*(20), L20311, doi:20310.21029/22005GL024296.

Han, S. C., R. D. Ray, and S. B. Luthcke (2007), Ocean tidal solutions in Antarctica from GRACE inter-satellite tracking data, *Geophys. Res. Lett.*, *34*(21).

Haran, T., J. Bohlander, T. Scambos, and M. Fahnestock (2005), MODIS mosaic of Antarctica (MOA) image map, edited, National Snow and Ice Data Center, Boulder, CO, USA.

Jenkins, A., H. F. J. Corr, K. W. Nicholls, C. L. Stewart, and C. S. M. Doake (2006), Interactions between ice and ocean observed with phase-sensitive radar near an Antarctic ice-shelf grounding line, *J. Glac.*, *52*(178), 325-346, doi:310.3189/172756506781828502.

Jenkins, A. C., Hugh F.J.; Nicholls, Keith W.; Stewart, Craig L.; Doake, Christopher S.M. (2006), Interactions between ice and ocean observed with phase-sensitive radar near an Antarctic ice-shelf grounding line, *Journal of Glaciology*, *52*(178), 325-346, doi:310.3189/172756506781828502.

King, M., and S. Aoki (2003), Tidal observations on floating ice using a single GPS receiver, *Geophys. Res. Lett.*, *30*(3), 1138, doi:1110.1029/2002GL016182.

King, M. A., and L. Padman (2005), Accuracy assessment of ocean tide models around Antarctica, *Geophys. Res. Lett.*, *32*, L23608, doi:23610.21029/22005GL023901.

King, M. A., N. T. Penna, P. J. Clarke, and E. C. King (2005), Validation of ocean tide models around Antarctica using onshore GPS and gravity data, *J. Geophys. Res.*, *110*, B08401, doi:08410.01029/02004JB003390.

King, M. A., C. S. Watson, N. T. Penna, and P. J. Clarke (2008), Subdaily signals in GPS observations and their effect at semiannual and annual periods, *Geophys. Res. Lett.*, *35*, L03302, doi:03310.01029/02007GL032252.

King, M. A., T. Murray, and A. M. Smith (2010), Non-linear responses of Rutford Ice Stream to semi-diurnal and diurnal tidal forcing, *J. Glac.*, *56*(195), 167-176, doi:110.3189/002214310791190848.

Knopoff, L., P. A. Rydelek, W. Zurn, and D. C. Agnew (1989), Observations of load tides at the South-Pole, *Phys. Earth Planet. Inter.*, *54*(1-2), 33-37.

Le Provost, C. (1991), Generation of overtides and compound tides (review), in *Tidal Hydrodynamics*, edited by B. B. Parker, pp. 269-296, John Wiley and Sons, New York.

Legresy, B., A. Wendt, I. Tabacco, F. Remy, and R. Dietrich (2004), Influence of tides and tidal current on Mertz Glacier, Antarctica, *Journal of Glaciology*, *50*(170), 427-435.

Lutjeharms, J. R. E., and C. C. Stavropoulos (1985), Tidal measurements along the Antarctic coastline, in *Oceanology of the Antarctic Continental Shelf*, edited by S. S. Jacobs, pp. 273-289, American Geophysical Union, Washington, D.C.

Lyard, F., F. Lefevre, T. Letellier, and O. Francis (2006), Modelling the global ocean tides: modern insights from FES2004, *Ocean Dynamics*, *56*(5-6), 394-415, doi:310.1007/s10236-10006-10086-x.

Makinson, K., and K. W. Nicholls (1999), Modeling tidal currents beneath Filchner-Ronne Ice Shelf and on the adjacent continental shelf: their effect on mixing and transport, *J. Geophys. Res.*, *104*(C6), 13449-13465.

Makinson, K., P. R. Holland, A. Jenkins, K. W. Nicholls, and D. M. Holland (2011), Influence of tides on melting and freezing beneath Filchner-Ronne Ice Shelf, Antarctica,, *Geophys. Res. Lett.*, *in press*, doi:10.1029/2010GL046462.

McCarthy, D. D., and G. Petit (2004), IERS Conventions (2003), IERS Technical Note 32, 127 pp, Verlag des Bundesamts für Kartographie und Geodäsie, Frankfurt am Main.

Melachroinos, S. A., J. M. Lemoine, P. Tregoning, and R. Biancale (2009), Quantifying FES2004 S-2 tidal model from multiple space-geodesy techniques, GPS and GRACE, over North West Australia, *J. Geodesy*, *83*(10), 915-923.

Moore, P., and M. A. King (2008), Antarctic ice mass balance estimates from GRACE: Tidal aliasing effects *Journal of Geophysical Research-Earth Surface*, *113*, F02005, doi:02010.01029/02007JF000871.

Munk, W. H., and D. E. Cartwright (1966), Tidal spectroscopy and prediction, *Philos. Proc. Roy. Soc.*, *259*(A1105), 533-581.

Murray, T., A. M. Smith, M. A. King, and G. P. Weedon (2007), Ice flow modulated by tides at up to annual periods at Rutford Ice Stream, West Antarctica, *Geophys. Res. Lett.*, *34*, L18503, doi:18510.11029/12007GL031207.

Padman, L., and C. Kottmeier (2000), High-frequency ice motion and divergence in the Weddell Sea, *J. Geophys. Res.*, *105*(C2), 3379-3400.

Padman, L., H. A. Fricker, R. Coleman, S. Howard, and L. Erofeeva (2002), A new tide model for the Antarctic ice shelves and seas, *Ann. Glaciol.*, *34*, 247-254.

Padman, L., M. King, D. Goring, H. Corr, and R. Coleman (2003), Ice shelf elevation changes due to atmospheric pressure variations, *J. Glac.*, *49*(167), 521-526.

Padman, L., and H. A. Fricker (2005), Tides on the Ross Ice Shelf observed with ICESat, *Geophys. Res. Lett.*, *32*(14), L14503, doi:14510.11029/12005GL023214.

Padman, L., S. Y. Erofeeva, and H. A. Fricker (2008), Improving Antarctic tide models by assimilation of ICESat laser altimetry over ice shelves, *Geophys. Res. Lett.*, *35*(22).

Pawlowicz, R., B. Beardsley, and S. Lentz (2002), Classical tidal harmonic analysis including error estimates in MATLAB using T_TIDE, *Computers and Geosciences*, *28*(8), 929-937.

Pedley, M., J. G. Paren, and J. R. Potter (1986), The tidal spectrum underneath Antarctic ice shelves, *J. Geophys. Res.*, *91*(C11), 13001-13009.

Penna, N. T., M. A. King, and M. P. Stewart (2007), GPS height time series: Short-period origins of spurious long-period signals, *J. Geophys. Res.*, *112*, B02402, doi:02410.01029/02005JB004047.

Potter, J. R., J. G. Paren, and M. Pedley (1985), Tidal behaviour under an Antarctic ice shelf, *Brit. Ant. Surv. Bull.*, *68*, 1-18.

Pugh, D. T. (1987), *Tides, surges and mean sea-level: a handbook for engineers and scientists*, 472 pp., John Wiley and Sons, Chichester.

Ray, R. D. (1999), A global ocean tide model from TOPEX/POSEIDON altimetry: GOT99.2, NASA Technical Memorandum, 58 pp.

Ray, R. D., R. J. Eanes, G. D. Egbert, and N. K. Pavlis (2001), Error spectrum for the global M_2 ocean tide, *Geophys. Res. Lett.*, *28*(1), 21-24, 10.1029/2000GL011674, 012001.

Ray, R. D. (2008), A preliminary tidal analysis of ICESat laser altimetry: Southern Ross Ice Shelf, *Geophys. Res. Lett.*, *35*, L02505, doi:02510.01029/02007GL032125.

Ray, R. D., S. B. Luthcke, and J. P. Boy (2009), Qualitative comparisons of global ocean tide models by analysis of intersatellite ranging data, *J. Geophys. Res.*, *114*.

Reeh, N., E. L. Christensen, C. Mayer, and O. B. Olesen (2003), Tidal bending of glaciers: a linear viscoelastic approach, *Annals of Glaciology, Vol 37*, *37*, 83-89.

Riedel, B., U. Nixdorf, M. Heinert, A. Eckstaller, and C. Mayer (1999), The response of the Ekstromisen (Antarctica) grounding zone to tidal forcing, *Ann. Glaciol.*, *29*, 239-242.

Rignot, E., L. Padman, D. R. MacAyeal, and M. Schmeltz (2000), Observation of ocean tides below the Filchner and Ronne Ice Shelves, Antarctica, using synthetic aperture radar interferometry: Comparison with tide model predictions, *J. Geophys. Res.*, *105*(C8), 19615-19630.

Riva, R. E. M., B. C. Gunter, T. J. Urban, B. L. A. Vermeersen, R. C. Lindenbergh, M. M. Helsen, J. L. Bamber, R. de Wal, M. R. van den Broeke, and B. E. Schutz (2009), Glacial Isostatic Adjustment over Antarctica from combined ICESat and GRACE satellite data, *Earth Plan. Sci. Lett.*, *288*(3-4), 516-523.

Sato, T., Y. Fukuda, Y. Aoyama, H. McQueen, K. Shibuya, Y. Tamura, K. Asari, and M. Ooe (2001), On the observed annual gravity variation and the effect of sea surface height variations, *Phys. Earth Planet. Inter.*, *123*(1), 45-63.

Scambos, T. A., T. M. Haran, M. A. Fahnestock, T. H. Painter, and J. Bohlander (2007), MODIS-based Mosaic of Antarctica (MOA) data sets: Continent-wide surface morphology and snow grain size, *Remote Sens. Environ.*, *111*(2-3), 242-257, doi:210.1016/j.rse.2006.1012.1020.

Schrama, E. J. O., B. Wouters, and D. A. Lavallee (2007), Signal and noise in Gravity Recovery and Climate Experiment (GRACE) observed surface mass variations, *J. Geophys. Res.*, *112*(B8).

Seo, K. W., C. R. Wilson, S. C. Han, and D. E. Waliser (2008), Gravity Recovery and Climate Experiment (GRACE) alias error from ocean tides, *J. Geophys. Res.*, *113*, B03405, doi:03410.01029/02006JB004747.

Shepherd, A., and N. R. Peacock (2003), Ice shelf tidal motion derived from ERS altimetry, *J. Geophys. Res.*, *108*(C6), 3198, doi:3110.1029/2001JC001152.

Smith, A. M. (1991), The use of tiltmeters to study the dynamics of Antarctic ice-shelf grounding lines, *Journal of Glaciology*, *37*(125), 51-58.

Sykes, H. J., T. Murray, and A. Luckman (2009), The location of the grounding zone of Evans Ice Stream, Antarctica, investigated using SAR interferometry and modelling, *Ann. Glac.*, *50*(52), 35-40, DOI: 10.3189/172756409789624292.

Thomas, I. D., M. A. King, and P. J. Clarke (2008), A Validation of Ocean Tide Models Around Antarctica Using GPS Measurements, in *Geodetic and Geophysical Observations in Antarctica*, edited by A. Capra and R. Dietrich, pp. 211-235, Springer.

Thomas, R. H. (2007), Tide-induced perturbations of glacier velocities, *Glob. Planet. Change*, *59*(1-4), 217-224, doi:210.1016/j.gloplacha.2006.1011.1017.

Tregoning, P., and T. A. Herring (2006), Impact of a priori zenith hydrostatic delay errors on GPS estimates of station heights and zenith total delays, *Geophys. Res. Lett.*, *33*(23), L23303, doi:23310.21029/22006GL027706.

van Dam, T. M., G. Blewitt, and M. B. Heflin (1994), Atmospheric Pressure Loading Effects on Global Positioning System Coordinate Determinations, *J. Geophys. Res.*, *99*(B12), 23939-23950.

Webb, F. H., and J. F. Zumberge (1995), An introduction to GIPSY/OASIS-II precision software for the analysis of data from the Global Positioning System, JPL Report, Jet Propulsion Laboratory, Pasadena, CA.

Yuan, L. G., X. L. Ding, P. Zhong, W. Chen, and D. F. Huang (2009), Estimates of ocean tide loading displacements and its impact on position time series in Hong Kong using a dense continuous GPS network, *J. Geodesy*, *83*(11), 999-1015, doi: 1010.1007/s00190-00009-00319-00190.

Zumberge, J. F., M. B. Heflin, D. C. Jefferson, M. M. Watkins, and F. H. Webb (1997), Precise point positioning for the efficient and robust analysis of GPS data from large networks, *J. Geophys. Res.*, *102*(B3), 5005-5017.

Tables

Table 1: Details of new sites. Note that due to close proximity of EE2B, EE4B and EE55 we only used EE55 in subsequent analysis. The EE4A record is partially grounded and is not used in the comparison with tide models. Coordinates are relative to the WGS84 ellipsoid.

Site	**Lat. (deg)**	**Long. (deg)**	**Height (m)**	**Duration (days)**	**Inference details**	**Local pressure data**
FR02	-80.9928	313.7116	99	117	P1/K1 and S2/K2 from CATS2008a	Y
FR03	-82.2088	301.4533	121	68	P1/K1 and S2/K2 from CATS2008a	Y
FR04	-80.1838	287.1175	109	39	P1/K1 and S2/K2 from FR05	Y
FR05	-78.2610	289.0971	79	370	none	Y
FR06	-76.6849	293.4864	67	55	P1/K1 and S2/K2 from FR05	Y
FR07	-75.8785	300.8505	48	214	none	Y
FR08	-77.6797	298.1000	46	18	none (response method)	Y
FR09	-79.1550	306.7999	55	307	none	Y
FR10	-77.1889	307.7945	36	78	P1/K1 and S2/K2 from mean of FR07 & FR09	Y

Site	Lat. (deg)	Long. (deg)	Height (m)	Duration (days)	Inference details	Local pressure data
EE2B	-76.3092	282.4159	182	94	P1/K1 and S2/K2 from FR05	N
EE4A	-76.5566	283.8026	115	83	-	-
EE4B	-76.6963	283.3138	126	84	P1/K1 and S2/K2 from FR05	N
EE55	-76.7589	284.5833	102	154	P1/K1 and S2/K2 from FR05	N
LAR1	-67.0133	298.4876	49	50	P1/K1 and S2/K2 from LAR2	Y
LAR2	-68.0004	295.7058	55	433	none	Y
LAR3	-68.5008	297.9982	29	64	P1/K1 and S2/K2 from LAR2	Y
SLGN	-67.9515	297.3309	53	38	P1/K1 and S2/K2 from LAR2	Y
SLGS	-67.9984	297.3122	55	36	P1/K1 and S2/K2 from LAR2	Y
J408	-68.5517	294.8451	98	41	P1/K1 and S2/K2 from LAR2	N

Table 2: Tide model details. T/P stands for TOPEX/Poseidon, ERS for European Remote Sensing Satellite, GFO for GEOSAT Follow On, ICESat for Ice, Cloud and land Elevation Satellite and TG for tide gauge data. Not all data sets include all constituents. We do not consider 2N2 here.

Model	Resolution	Data assimilated	Diurnal/Semi-diurnal constituents	Nonlinear constituents
TPXO7.2 [*Egbert et al.*, 2009]	0.25 x 0.25°	GRACE, ERS, T/P, TG (high latitudes)	M2, S2, N2, K2, K1, O1, P1, Q1	M4, MS4, MN4
GOT4.7 [*Ray*, 1999]	0.5 x 0.5°	TOPEX, ERS+GFO (high latitude/shallow seas), ICESat (Weddell & Ross Sea ice shelves)	M2, S2, N2, K2, K1, O1, P1, Q1, S1	M4
FES2004 [*Lyard et al.*, 2006]	0.125 x 0.125 °	T/P, ERS, TG (not high latitude)	M2, S2, N2, 2N2, K2, K1, O1, P1, Q1, S1	M4
CATS2008a [*Padman et al.*, 2002]	4km (~0.12^{o}x0.04^{o} at 72^{o}S)	T/P, ICESat (Antarctic Ice Shelves), TG (Antarctic)	M2, S2, N2, 2N2, K2, K1, O1, P1, Q1	none

Table 3: Misfit RMS (σ_k) and RSS for all sites, units are in centimeters, with *N*=31 in Eq 1.

	TPXO7.2*	FES2004	CATS2008a*	GOT4.7
M2	8.0	27.0	7.3	28.2
S2	5.9	18.2	5.0	18.6
O1	3.2	7.1	2.7	10.2
K1	3.9	9.3	3.5	10.0
N2	2.5	5.2	2.9	4.8
K2	2.3	6.0	1.7	5.7
P1	2.2	3.1	1.7	3.5
Q1	1.3	1.9	1.4	2.1
RSS	11.9	35.6	10.7	37.6

* These models assimilate a subset of the data

Table 4: As for Table 3, but after excluded the two sites with worst agreement for each model

	TPXO7.2*	FES2004	CATS2008a*	GOT4.7
M2	5.2	8.0	4.8	5.2
S2	4.1	5.0	4.1	4.3
O1	2.4	4.2	1.7	6.8
K1	3.2	5.1	2.9	5.1
N2	1.5	1.8	2.0	1.6
K2	1.6	1.3	1.3	1.3
P1	1.9	1.7	1.3	1.8
Q1	1.0	1.0	1.1	1.0
RSS	8.3	11.9	7.8	11.3

* These models assimilate a subset of the data

Table 5: S1 amplitudes and phases. Uncertainties are given at their 95% confidence interval.

Site	Observed (cm, °)	FES2004 (cm, °)
LAR2	1.2±0.3 356±17	0.6 345
FR05	0.6±0.4 9±37	0.8 37
FR07	0.6±0.3 329±27	0.2 76
FR09	0.3±0.3 14±58	0.8 13
PALM	0.3±0.2 341±39	-

Table 7: Amplitudes and Greenwich phases for observed and modeled M4, MS4 and MN4. TPXO7.2 values for EE2B and EE4B have been taken from the location of EE55. MS4 and MN4 are not available for FES2004. Phases are not shown when amplitude is 0.0 cm

		M4		MS4		MN4	
		Amp. (cm)	Phs. (°)	Amp. (cm)	Phs. (°)	Amp. (cm)	Phs. (°)
FR02	Obs.	0.7±0.01	186±3	0.5±0.01	216±4	2.0±0.01	152±11
	TPXO7.2	0.4	128	0.4	164	0.2	80
	FES2004	0.0	-				
FR03	Obs.	2.4±0.4	170±9	0.5±0.3	247±31	1.0±0.4	127±19
	TPXO7.2	0.9	147	0.4	214	0.4	100
	FES2004	0.5	31				
FR04	Obs.	2.6±0.5	6±10	1.2±0.4	32±20	1.4±0.5	316±19
	TPXO7.2	0.5	20	3.0	67	0.3	301
	FES2004	1.2	323				
FR05	Obs.	1.9±0.1	341±4	1.1±0.1	353±7	0.7±0.1	309±11
	TPXO7.2	0.4	28	1.3	88	0.2	317
	FES2004	1.6	239				
FR06	Obs.	0.6±0.4	338±34	0.3±0.3	5±52	0.4±0.3	298±43
	TPXO7.2	0.2	66	0.7	174	0.0	-
	FES2004	0.9	235				

		M4		MS4		MN4	
		Amp. (cm)	Phs. (°)	Amp. (cm)	Phs. (°)	Amp. (cm)	Phs. (°)
FR07	Obs. TPXO7.2 FES2004	0.4±0.1 0.1 0.0	60±13 159 -	0.2±0.1 1.0	161±18 235	0.2±0.1 0.1	0±27 127
FR09	Obs. TPXO7.2 FES2004	2.6±0.2 0.3 1.4	180±3 196 100	1.0±0.1 1.4	235±8 266	1.1±0.2 0.1	131±8 120
FR10	Obs. TPXO7.2 FES2004	10.4±0.2 0.2 1.0	76±9 108 62	1.3±0.2 1.0	125±10 226	0.4±0.2 0.2	27±30 79
EE2B	Obs. TPXO7.2 FES2004	0.9±0.2 0.4 2.0	336±14 42 232	0.5±0.3 1.2	358±26 124	0.2±0.3 0.0	342±49 -
EE4A	Obs. TPXO7.2 FES2004	1.7±0.4 0.4 1.9	178±12 42 232	3.0±0.4 1.2	211±6 124	0.1±0.3 0.1	137±121 335
EE4B	Obs. TPXO7.2 FES2004	1.5±0.01 0.4 2.0	337±1 42 232	1.0±0.01 1.2	330±1 124	0.5±0.01 0.1	315±3 335

		M4		MS4		MN4	
		Amp. (cm)	Phs. (°)	Amp. (cm)	Phs. (°)	Amp. (cm)	Phs. (°)
EE55	Obs. TPXO7.2 FES2004	1.6±0.1 0.4 1.8	340±2 42 231	1.0±0.1 1.2	335±4 124	0.6±0.1 0.1	318±8 335
LAR1	Obs. TPXO7.2 FES2004	1.2±0.2 0.2 0.3	257±10 347 149	0.3±0.2 1.6	243±34 187	0.6±0.3 0.0	208±19 -
LAR2	Obs. TPXO7.2 FES2004	1.4±0.2 0.2 0.5	240±6 319 132	1.1±0.2 2.6	232±7 173	0.7±0.2 0.1	216±12 211
LAR3	Obs. TPXO7.2 FES2004	1.0±0.3 0.2 0.3	229±13 151 101	0.3±0.2 1.4	225±37 160	0.5±0.2 0.0	171±25 -
SLGN	Obs. TPXO7.2 FES2004	1.3±0.4 0.2 0.4	235±18 329 127	0.7±0.4 1.9	234±29 171	0.8±0.4 0.0	204±27 -
SLGS	Obs. TPXO7.2 FES2004	1.3±0.5 0.2 0.4	234±19 329 126	0.6±0.4 1.9	228±33 171	0.8±0.5 0.0	208±29 -

		M4		MS4		MN4	
		Amp. (cm)	Phs. (°)	Amp. (cm)	Phs. (°)	Amp. (cm)	Phs. (°)
J408	Obs. TPXO7.2 FES2004	1.3±0.5 0.2 0.5	213±17 312 128	1.6±0.4 2.8	208±16 172	0.4±0.4 0.1	202±59 212

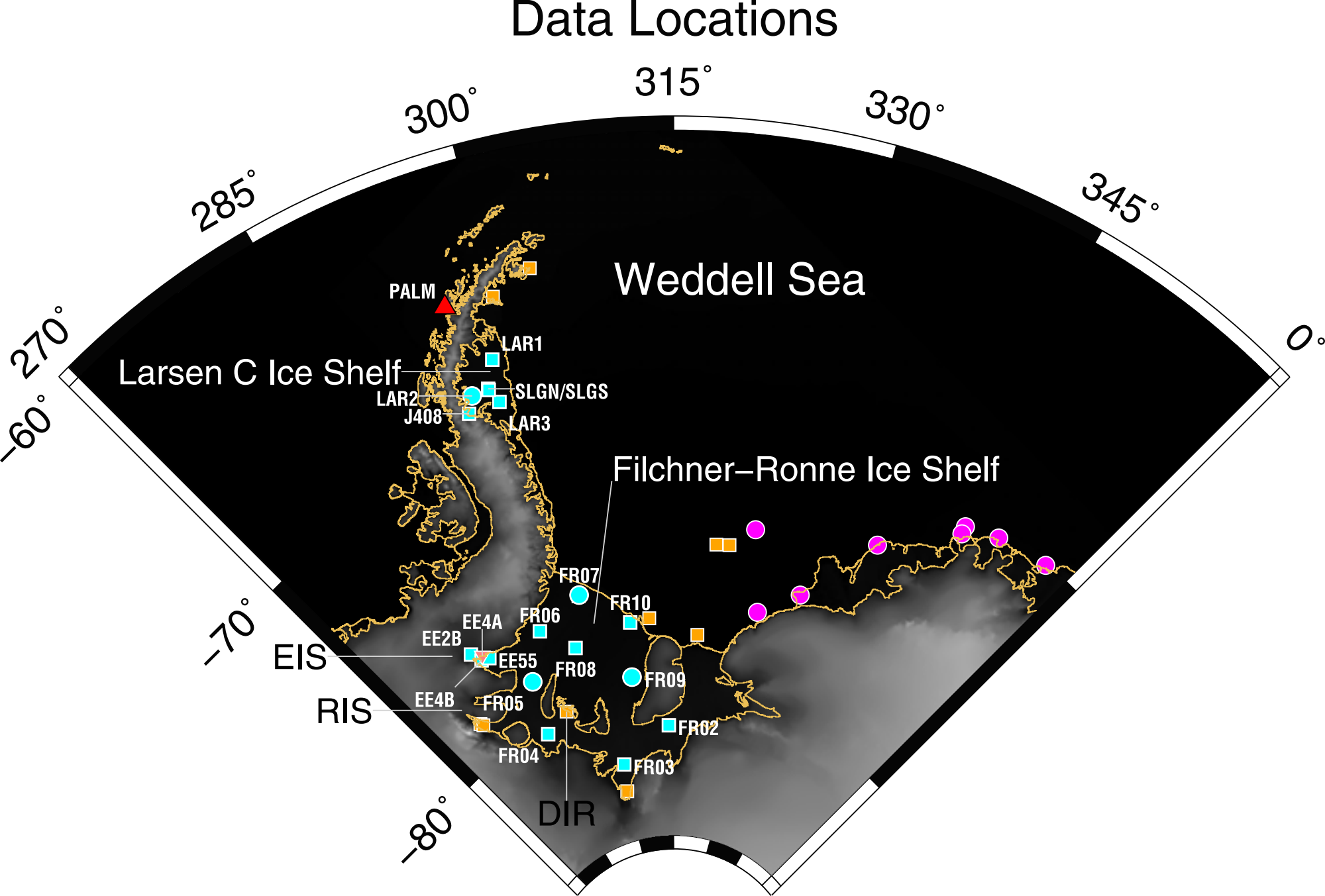
Data Locations
315°
300°
330°
285°
345°
270°
0°
−60°
−70°
−80°
Weddell Sea
Larsen C Ice Shelf
Filchner–Ronne Ice Shelf
PALM
LAR1
LAR2
SLGN/SLGS
J408
LAR3
FR07
FR10
FR06
EE4A
EE2B
EIS
EE55
FR08
FR09
RIS
EE4B
FR05
FR02
FR04
FR03
DIR

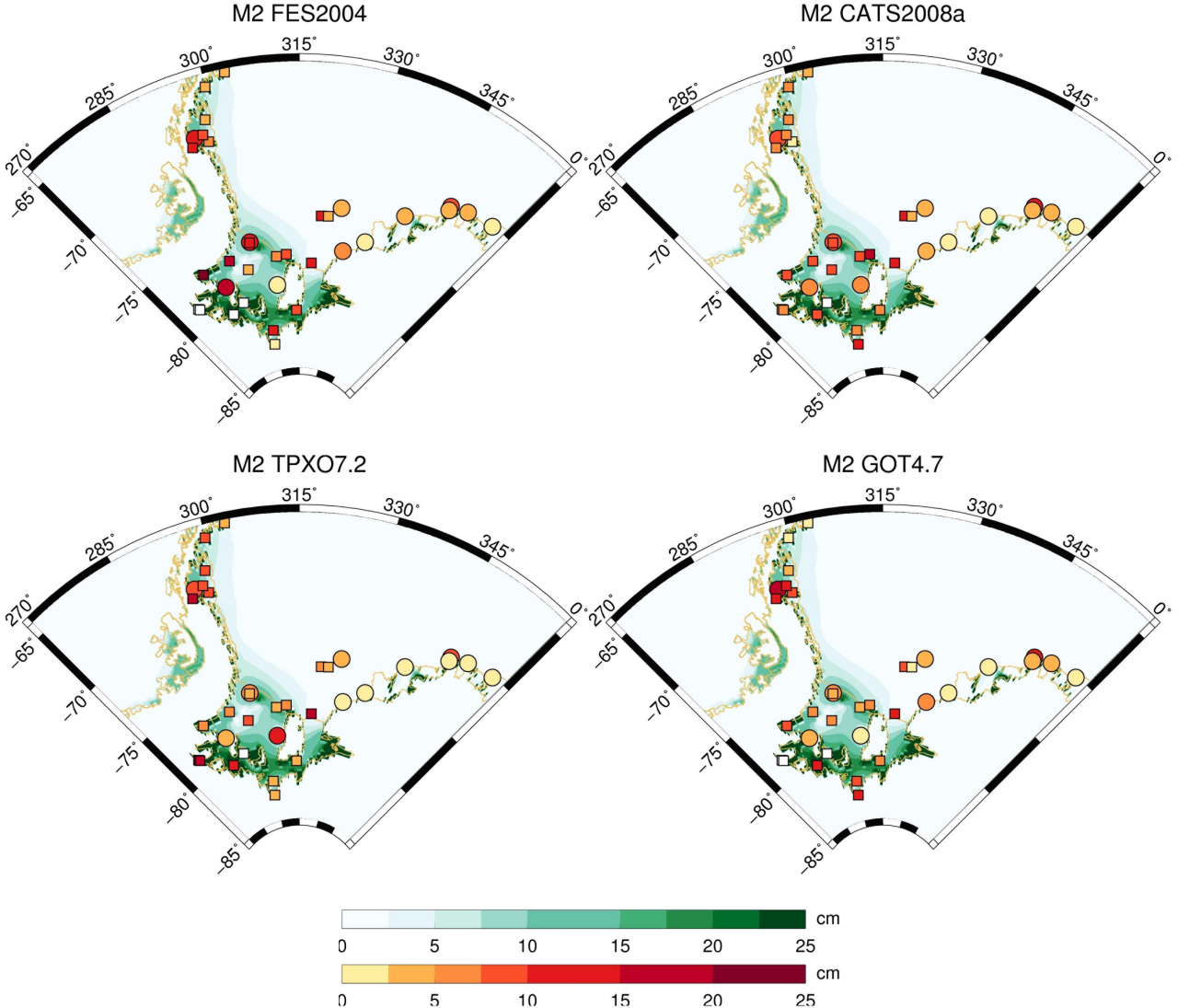
M2 FES2004
M2 CATS2008a
M2 TPXO7.2
M2 GOT4.7
300°
315°
330°
345°
0°
285°
270°
-65°
-70°
-75°
-80°
-85°
cm
0
5
10
15
20
25
cm
0
5
10
15
20
25

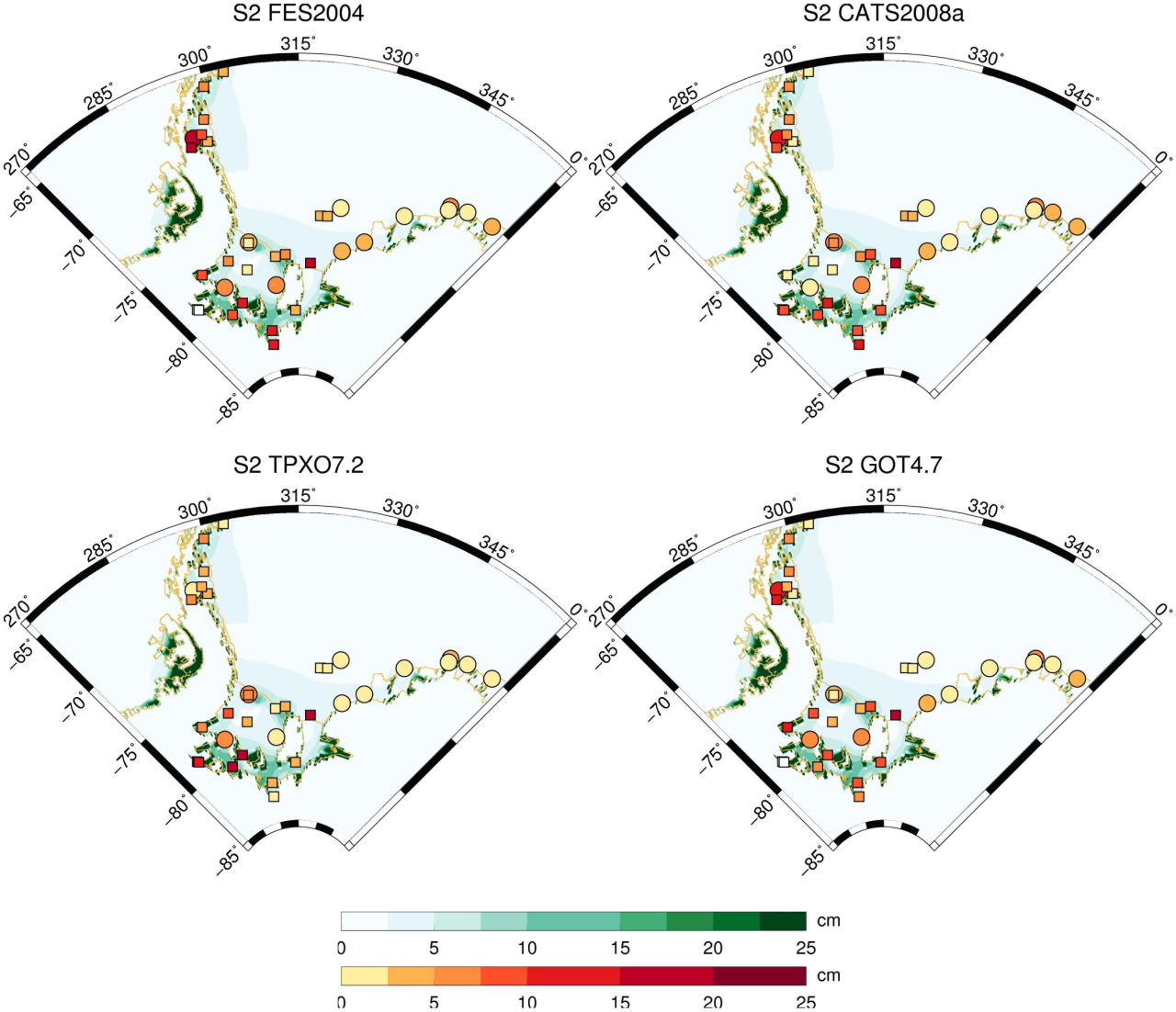
S2 FES2004
S2 CATS2008a
S2 TPXO7.2
S2 GOT4.7
300°
315°
330°
345°
0°
285°
270°
-65°
-70°
-75°
-80°
-85°
cm
0
5
10
15
20
25
cm
0
5
10
15
20
25

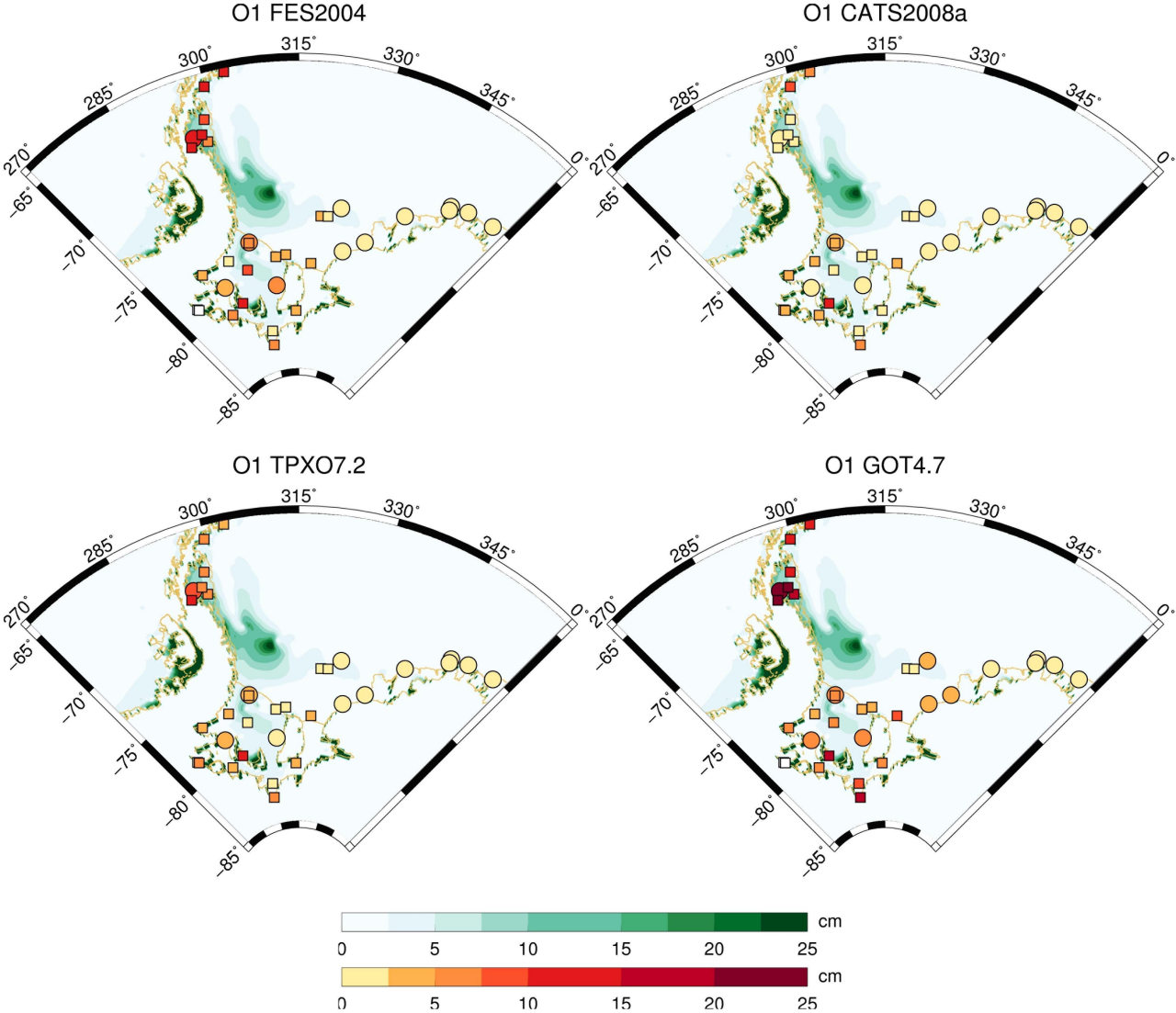
O1 FES2004
O1 CATS2008a
O1 TPXO7.2
O1 GOT4.7
300°
315°
330°
345°
0°
285°
270°
-65°
-70°
-75°
-80°
-85°
cm
0
5
10
15
20
25
cm
0
5
10
15
20
25

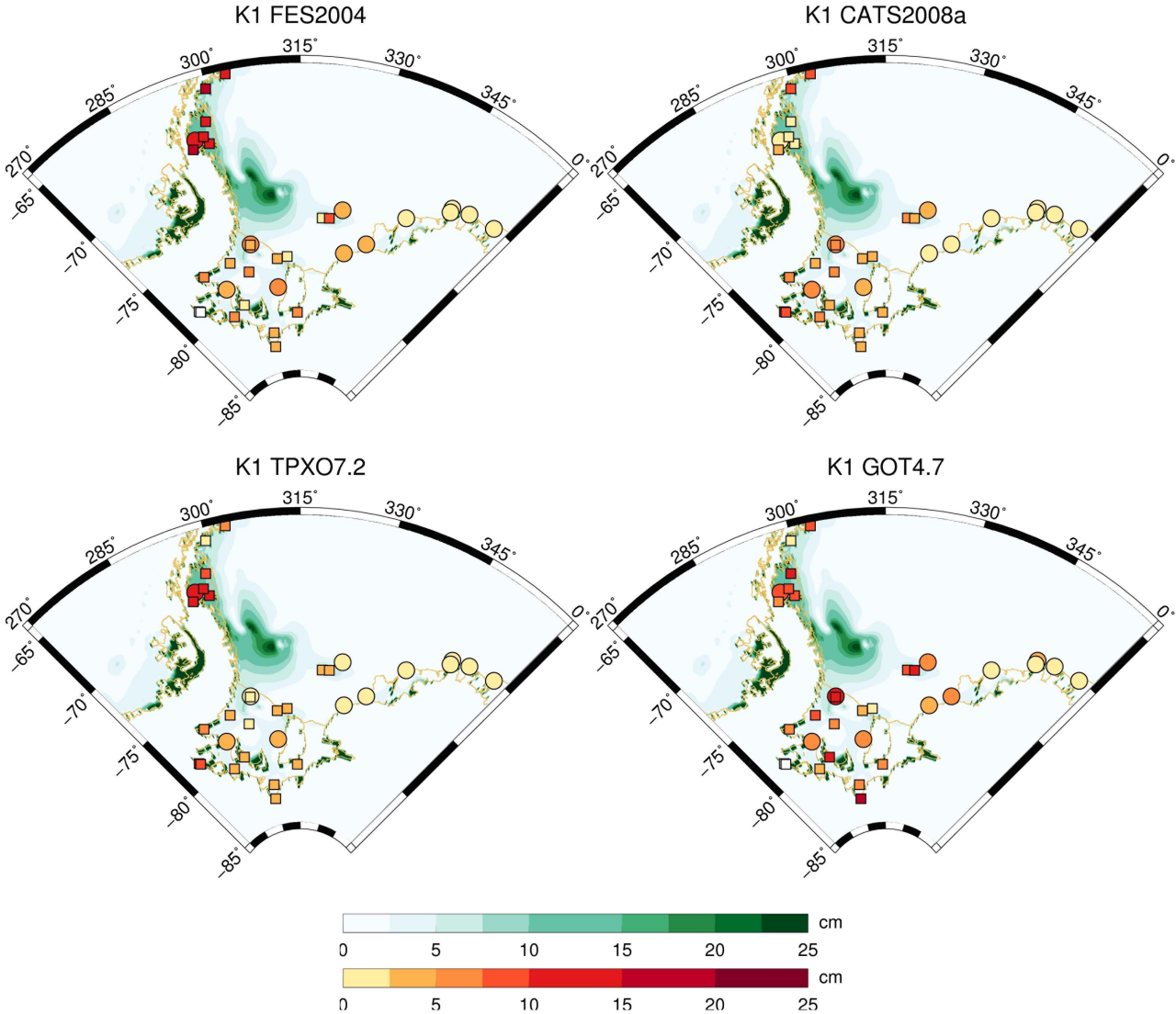
K1 FES2004
K1 CATS2008a
K1 TPXO7.2
K1 GOT4.7
300°
315°
330°
345°
0°
285°
270°
-65°
-70°
-75°
-80°
-85°
cm
0
5
10
15
20
25
cm
0
5
10
15
20
25

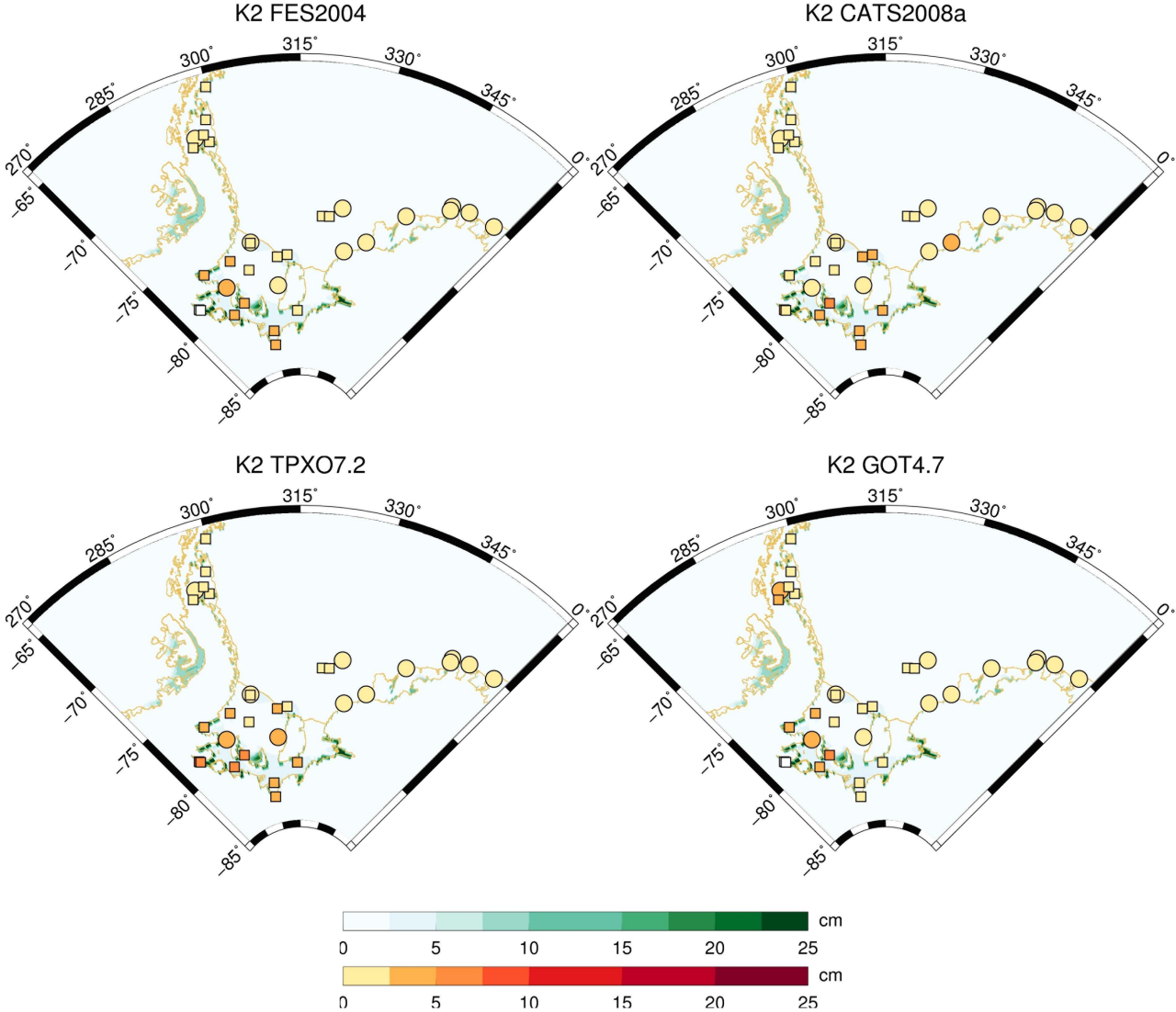
K2 FES2004
K2 CATS2008a
K2 TPXO7.2
K2 GOT4.7
300°
315°
330°
345°
0°
285°
270°
-65°
-70°
-75°
-80°
-85°
cm
0
5
10
15
20
25
cm
0
5
10
15
20
25

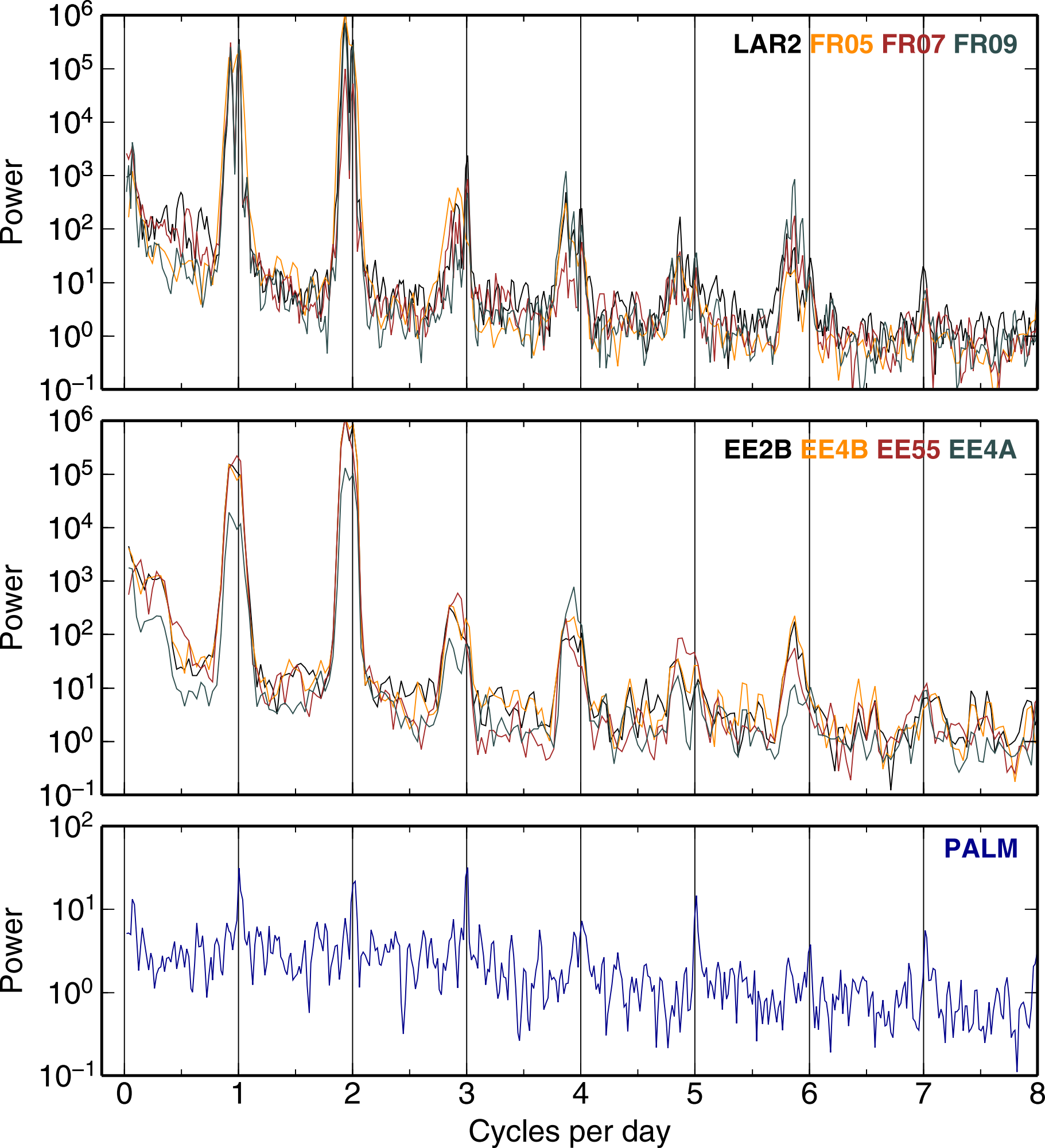
LAR2 FR05 FR07 FR09
EE2B EE4B EE55 EE4A
PALM
Power
Power
Power
Cycles per day
0
1
2
3
4
5
6
7
8

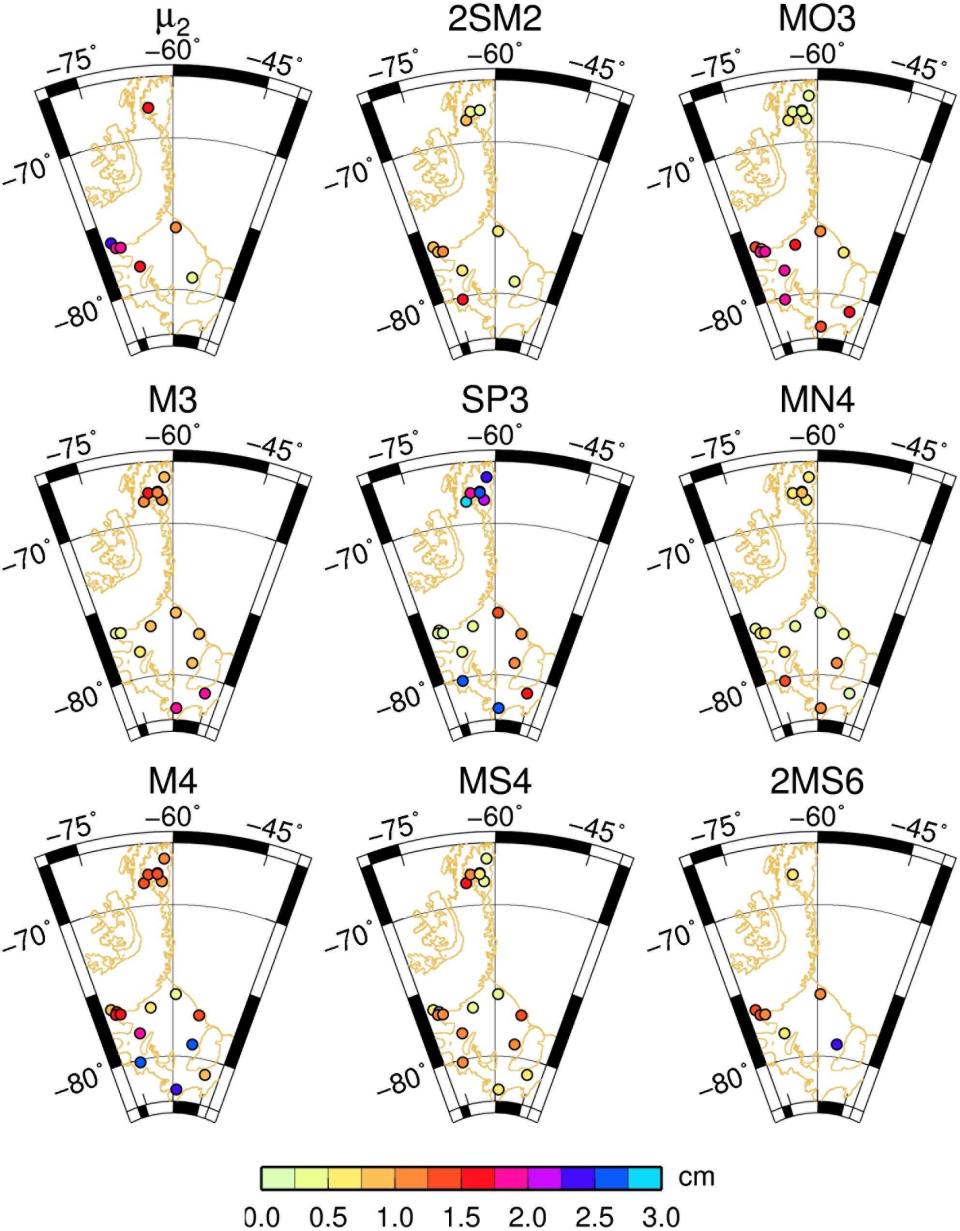
μ2
2SM2
MO3
M3
SP3
MN4
M4
MS4
2MS6
−75°
−60°
−45°
−70°
−80°
cm
0.0
0.5
1.0
1.5
2.0
2.5
3.0